

1 **NO<sub>2</sub> and HCHO measurements in Korea from 2012 to 2016 from Pandora Spectrometer Instruments**  
2 **compared with OMI retrievals and with aircraft measurements during the KORUS-AQ campaign**

3 **Jay Herman<sup>1</sup>, Elena Spinei<sup>2</sup>, Alan Fried<sup>3</sup>, Jhoon Kim<sup>4</sup>, Jae Kim<sup>5</sup>, Woogyung Kim<sup>3</sup>, Alexander Cede<sup>6</sup>, Nader**  
4 **Abuhassan<sup>1</sup>, Michal Segal-Rozenhaimer<sup>7,8</sup>**

5

6

7

8

9

10

11

12

13

14

15

16

17

18 **Correspondence email: [jay.r.herman@nasa.gov](mailto:jay.r.herman@nasa.gov)**

19 **<sup>1</sup>University of Maryland Baltimore County JCET**

20 **<sup>2</sup>Virginia Polytechnic Institute and State University, Blacksburg, VA 24061, USA**

21 **<sup>3</sup>Institute of Arctic & Alpine Research, University of Colorado, Boulder, Colorado**

22 **<sup>4</sup>Dept. of Atmospheric Sciences, Yonsei University, Seoul Korea**

23 **<sup>5</sup>Department of Atmospheric Science, Pusan University, Busan, Korea**

24 **<sup>6</sup>Goddard Earth Sciences Technology & Research (GESTAR) Columbia, Columbia, MD 21046, USA**

25 **<sup>7</sup>Earth Science Division, NASA Ames, Mountain View, California**

26 **<sup>8</sup>Bay Area Environmental Research Institute, Petaluma, California**

27

28

29 **NO<sub>2</sub> and HCHO measurements in Korea from 2012 to 2016 from Pandora Spectrometer Instruments**  
30 **compared with OMI retrievals and with aircraft measurements during the KORUS-AQ campaign**

31  
32 **Abstract**

33  
34 Nine Pandora Spectrometer Instruments (PSI) were installed at 8 sites in South Korea as part of  
35 the KORUS-AQ (Korea U.S.-Air Quality) field study integrating information from ground, aircraft,  
36 and satellite measurements for validation of remote sensing air-quality studies. The PSI made  
37 direct-sun measurements of total vertical column NO<sub>2</sub>, C(NO<sub>2</sub>), with high precision (0.05 DU,  
38 where 1DU = 2.69x10<sup>16</sup> molecules/cm<sup>2</sup>) and accuracy (0.1 DU) that were retrieved using  
39 spectral fitting techniques. Retrieval of Formaldehyde (HCHO) total column amounts were also  
40 obtained at five sites using the recently improved PSI optics. The HCHO retrievals have with  
41 high precision, but possibly lower accuracy than for NO<sub>2</sub> because of uncertainty about the  
42 optimum spectral window for all ground-based and satellite instruments. PSI direct-sun  
43 retrieved values of C(NO<sub>2</sub>) and C(HCHO) are always significantly larger than OMI (AURA satellite  
44 Ozone Monitoring Instrument) retrieved C(NO<sub>2</sub>) and C(HCHO) for the OMI overpass local times  
45 (LT = 13.5 ± 0.5 hours). In urban areas, PSI C(NO<sub>2</sub>) 30-day running averages are at least a factor  
46 of two larger than OMI averages. Similar differences are seen for C(HCHO) in Seoul and nearby  
47 surrounding areas. Late afternoon values of C(HCHO) measured by PSI are even larger, implying  
48 that OMI early afternoon measurements underestimate the effect of poor air quality on human  
49 health. The primary cause of the OMI underestimate is the large OMI field of view (FOV) that  
50 includes regions containing low values of pollutants. In relatively clean areas, PSI and OMI are  
51 more closely in agreement. C(HCHO) amounts were obtained for five sites, Yonsei University in  
52 Seoul, Olympic Park, Taehwa Mtn., Amnyeondo, and Yeosu. Of these the largest amounts of  
53 C(HCHO) were observed at Olympic Park and Taehwa Mountain, surrounded by significant  
54 amounts of vegetation. Comparisons of PSI C(HCHO) results were made with the Compact  
55 Atmospheric Multispecies Spectrometer CAMS during overflights on the DC-8 aircraft for  
56 Taehwa Mtn and Olympic Park. In all cases, PSI measured substantially more C(HCHO) than  
57 obtained from integrating the CAMS altitude profiles. PSI C(HCHO) at Yonsei University in Seoul  
58 frequently reached 0.6 DU and occasionally exceeded 1.5DU. The semi-rural site, Mt. Taehwa,  
59 frequently reached 0.9 DU and occasionally exceeded 1.5DU. Even at the cleanest site,  
60 Amnyeondo, HCHO occasionally exceeded 1 DU.

61  
62 Keywords: Pandora, KORUS-AQ, NO<sub>2</sub>, HCHO, Formaldehyde, Korea

63

## 64 1 Introduction

65 The purpose of this paper is to present the retrieved amounts of nitrogen dioxide and  
66 formaldehyde, NO<sub>2</sub> and HCHO, obtained from Pandora Spectrometer instruments (PSI) direct-sun  
67 observations during the KORUS-AQ campaign (Korea US Air Quality: May – June 2016). Quoting from a  
68 NASA website: “Korea U.S.-Air Quality (KORUS-AQ) is a joint field study between NASA and the Republic  
69 of Korea to advance the ability to monitor air pollution from space. The campaign will assess air quality  
70 across urban, rural and coastal South Korea using observations from aircraft, ground sites, ships and  
71 satellites to test air quality models and remote sensing methods. Findings will help develop observing  
72 systems using models and data to improve air quality assessments for decision makers.” A thorough  
73 description of the KORUS-AQ campaign and its motivations is given in a pre-campaign white paper,  
74 [https://espo.nasa.gov/korus-aq/content/KORUS-AQ\\_White\\_Paper](https://espo.nasa.gov/korus-aq/content/KORUS-AQ_White_Paper).

75 Assessing air quality in South Korea is of interest because of the levels of pollution arising from  
76 high densities of population and intense industrial activity associated with the production of NO<sub>2</sub>.  
77 Recent measurements of surface concentrations of NO<sub>2</sub> and comparisons with satellite data  
78 demonstrate the need for high quality ground-based measurements to augment satellite observations  
79 (Kim et al., 2017; Jung et al., 2017). The driving reason behind the interest is the effect of elevated levels  
80 of NO<sub>2</sub> in Korea on human health (Kim and Song, 2017 and references therein). Measurements of N O<sub>2</sub>  
81 from aircraft have been used to obtain altitude profiles to compare with data obtained from fixed site  
82 measurements and to obtain a national scale estimate of pollutant exposure (Lee et al., 2015; Kim and  
83 Song, 2017).

84 In addition to NO<sub>2</sub>, PSI measurements were used to assess the amount of Formaldehyde (HCHO)  
85 present in the air. This is important because of HCHO potential impact on health (Zhang et al., 2013, )  
86 and because it plays a strong role in tropospheric reactions leading to the formation of boundary layer  
87 ozone. Sources of HCHO are from atmospheric reactions with volatile organic compounds (VOC) emitted  
88 from ground sources and industrial activities (Lee et al., 2009). A previous paper describes HCHO  
89 retrievals from a PSI located at Yonsei University in Seoul using a similar spectral fitting retrieval  
90 algorithm used in the current study (Park et al., 2018), but using a different wavelength fitting range,  
91 335 – 358 nm instead of 332 – 359 nm used in this study. The choice of spectral fitting window is  
92 discussed in Spinei et al. (2018).

93 As part of the KORUS-AQ campaign, a network of nine PSI was installed in Korea at 8 locations  
94 (Fig. 1 and Table 1). Five of the sites were selected to be “down-wind” from Seoul, an extremely NO<sub>2</sub>  
95 polluted area. The intent of the network was to integrate direct-sun column density observations of  
96 NO<sub>2</sub> and HCHO into a multi-perspective framework of observations including ground-based, satellite,  
97 and airborne measurements of air quality. Viewing air quality through these multiple perspectives is  
98 important for connecting observations from future geostationary satellites to air quality networks such  
99 that conditions both at the surface and aloft can be better understood and represented across  
100 unmonitored areas. The data are especially important for computer models used for forecasts and  
101 decision making. Five of the KORUS-AQ PSI had recently improved optics that permitted retrieval of total  
102 vertical column formaldehyde (C(HCHO)). Part of the network was installed in April 2015, a year before

103 the start of the campaign. Three PSI continue to operate in Korea, one each, in Busan and Seoul since  
104 2012, and one in Gwangju operating since April 2015.

105  
106 Measurements of daytime total columns in Dobson Units, where  $1 \text{ DU} = 2.69 \times 10^{16}$   
107 molecules/cm<sup>2</sup>, C(NO<sub>2</sub>), C(O<sub>3</sub>) and C(HCHO) are obtained every 80 seconds, which enables the PSI to  
108 show rapid short term (minutes to hours) variations in most locations with significant pollution (e.g.,  
109 C(NO<sub>2</sub>) > 0.2 DU). PSI measurements of the visible and UV wavelengths are obtained separately (40  
110 seconds each). A visible wavelength blocking filter, U340, reduces stray light for UV measurements.

111

Table 1 KORUS-AQ Locations (South to North)

Locations	Alt(m)	Latitude	Longitude
Gwangju	33	35.2260°N	126.8430°W
Busan	228	35.2353°N	129.0825°W
Anmyeondo	41	36.5380°N	126.3300°W
Taehwa Mtn	160	37.3123°N	127.3106°W
Yeoju-1 & 2	90	37.3385°N	127.4895°W
Songchon	49	37.4100°N	127.5600°W
Olympic Park	26	37.5232°N	127.1260°W
Seoul	181	37.5644°N	126.9340°W

112

113 Details on the Pandora spectrometer instrument can be found in Herman et al., (2009 and 2015)  
114 as well as a NASA Pandora website

115 [https://avdc.gsfc.nasa.gov/pub/DSCOVER/Pandora/Web\\_Pandora/index.html](https://avdc.gsfc.nasa.gov/pub/DSCOVER/Pandora/Web_Pandora/index.html) and the data used are  
116 available from <https://avdc.gsfc.nasa.gov/pub/DSCOVER/Pandora/DATA/KORUS-AQ/>

117

118 The PSI consists of a small Avantes low stray light spectrometer (280 – 525 nm with 0.6 nm  
119 spectral resolution with 4 times oversampling) connected to an optical head by a 400 micron single  
120 strand fiber optic cable. The spectrometer is temperature stabilized at 20°C (68°F) inside of a weather  
121 resistant container. The optical head consists of a collimator and lens giving rise to a 1.6° FOV (field of  
122 view) FWHM (Full Width Half Maximum) with light passing through two filter wheels containing  
123 diffusers, a UV340 filter (blocks visible light), neutral density filters, and an opaque position (dark  
124 current measurement). When the diffuser is used, the FOV is increased to over 2°. The optical head is  
125 connected to a small suntracker capable of accurately following the sun's center using software running  
126 on a small computer-data logger contained in a weatherproof outer box along with the spectrometer in  
127 a second inner temperature controlled box. The PSI is capable of obtaining C(NO<sub>2</sub>), C(HCHO) and C(O<sub>3</sub>)  
128 amounts sequentially over a period of 80 seconds including two dark current determinations. The  
129 integration time for NO<sub>2</sub> in bright sun is about 4 milli-seconds that is repeated and averaged for 20  
130 seconds (up to 4000 measurements) to obtain very high signal to noise ratios and very high precision  
131 (precision < 0.01 DU). Similar comments apply to C(O<sub>3</sub>), but not to C(HCHO), since formaldehyde  
132 absorption spectrum is mixed in with absorption from NO<sub>2</sub> and O<sub>3</sub>. This causes cross-correlation effects  
133 in the retrieval algorithm that make C(HCHO) retrievals sensitive to the selection of the wavelength

134 range. The main source of noise in the measurement comes from the presence of clouds or haze in the  
135 FOV, which increases the exposure time and reduces the number of measurements in 20 seconds.

136  
137 The retrieval algorithm is based a direct-sun spectral fitting method similar to the well-accepted  
138 DOAS (Differential Optical Absorption Spectroscopy, Platt, et al., 1979 and Platt, 1994 ). NO<sub>2</sub> absorption  
139 cross sections were obtained from the laboratory measurements of Vandaele et al., 1998, and HCHO  
140 cross sections from Meller and Moortgat (2000). The PSI reference solar spectrum is constructed from a  
141 high resolution extraterrestrial spectrum from 270 nm to 1000 nm merged from different sources  
142 (Bernhard et al. (2004). Solar spectrum sources are from: Kurucz (2005) normalized to Thuillier et al.  
143 (2004), SUSIM/Atlas-3 spectrum (VanHoosier et al., 1996), and the spectrum from Gueymard (2004).  
144 One of the advantages of using direct-sun observations is the accurate conversion to vertical column  
145 based on a geometric calculation of the slant path air mass factor AMF for a known solar zenith angle  
146 SZA is with a slight correction to the function Secant(SZA) (Herman et al., 2009 eqn. 3). A complete  
147 description of the retrieval algorithms and PSI operations are given in the PSI software manual (Cede,  
148 2017). Accuracy in the DOAS-type retrieval is obtained using careful measurements of the  
149 spectrometer's slit function, wavelength calibration, knowledge of atmospheric absorption cross  
150 sections, and the solar spectrum at the top of the atmosphere. Accuracy for C(NO<sub>2</sub>) has been estimated  
151 to be ±0.05 DU. A recent addition of anti-reflection coatings to the PSI optics has improved accuracy and  
152 precision by reducing the residuals associated with spectral fitting using trace gas absorption cross  
153 sections. The reduced residuals are necessary for the retrieval of formaldehyde and bromine oxide that  
154 absorb in spectral regions dominated by ozone and NO<sub>2</sub>. Other DOAS-type measurements have been  
155 made in Korea based on observations of sky radiance ratios (e.g., Multi Axis MAX-DOAS: Kanaya, et al.,  
156 2014) and direct-sun DOAS using a PSI in Seoul, Korea (Park et al., 2018).

157  
158 This paper discusses the distribution of C(NO<sub>2</sub>) and C(HCHO) over Korea at the sites where the  
159 PSI were located (Fig. 1). Section 2 shows the amounts of NO<sub>2</sub> observed by PSIs at the 8 KORUS-AQ  
160 sites. Section 3 discusses the diurnal variation of NO<sub>2</sub>. Section 4 looks at longer term changes in NO<sub>2</sub>  
161 obtained from PSIs that were deployed before the beginning of the KORUS-AQ campaign. Section 5  
162 evaluates the disagreement with Ozone Monitoring Instrument (OMI) satellite C(NO<sub>2</sub>) retrievals (Kramer  
163 et al., 2008). Section 6 compared PSI C(NO<sub>2</sub>) retrievals with the aircraft overpass retrievals from the  
164 4STAR instrument (Segal-Rozenhaimer et al., 2014). Section 6 discusses retrievals of C(HCHO) amounts  
165 for five PSI sites, the diurnal variation of C(HCHO), and comparisons with the Compact Atmospheric  
166 Multispecies Spectrometer CAMS (Richter et al., 2015) from DC-8 aircraft overflights of 5 PSI sites.

167  
168

## 169 **2 NO<sub>2</sub> during the KORUS-AQ Campaign (May – June 2016)**

170 An example of NO<sub>2</sub> retrieval from two independently calibrated Pandoras that were initially  
171 located at the same site (Yeoju, Korea, 37.3385°N, 127.4895°W) are compared in Fig. 2a showing that  
172 the difference in C(NO<sub>2</sub>) amount is less than 0.05 DU even in the presence of thin afternoon clouds (Fig.  
173 2b) that decrease the measured solar irradiance by more than a factor of 2. Though Yeoju is a relatively

174 clean site in Korea (located to the southeast of Seoul Lat=37.5644°N, Long=126.934°W), C(NO<sub>2</sub>) amounts  
175 frequently reach moderately high values (e.g., 1 DU on 3 June 2016), and occasionally even higher (2-3  
176 DU). However, Yeosu has much less C(NO<sub>2</sub>) compared to Seoul, less than 30 km distant, where PSI  
177 measurements were found to reach over 3 DU (Fig. 3) during the campaign period from mid-April to  
178 early June, 2016. Typical C(NO<sub>2</sub>) amounts are 0.3 to 0.5 DU in polluted regions.

179  
180 In a manner similar to Fig. 2a, C(NO<sub>2</sub>) amounts can show large variability from day-to-day and  
181 intraday, as well as between different sites. The largest amounts of C(NO<sub>2</sub>) are in the north (Seoul and  
182 Olympic Park) associated with the largest population and industry concentrations, while the southern  
183 cities of Busan and Gwangju have smaller amounts of C(NO<sub>2</sub>). The smallest C(NO<sub>2</sub>) amounts are at  
184 Anmyeondo (an island on west coast of Korea 42 km south of Seoul, usually not downwind of Seoul),  
185 and Songchon to the east of Seoul.

186  
187 Figure 2b shows the effect of thin clouds in terms of reduced measured count rates for a single  
188 spectrometer pixel near 500 nm showing a near noon count rate of  $1.26 \times 10^7$  counts/second followed  
189 by a reduced count rate as clouds move in front of the sun. The cloud plus aerosol cover estimate is  
190 from the same date 3 June 2016 as the C(NO<sub>2</sub>) amounts shown in Fig.2a. The effect of thin clouds for  
191 C(NO<sub>2</sub>) retrieval (Fig. 2a) is increased noise (reduced precision) with a very small impact on accuracy.  
192 There are two effects on PSI observations to consider in association with thin clouds. First, is multiple  
193 scattering within the cloud affecting the optical path and effective air mass factor AMF. This has a very  
194 small effect on AMF, since most of the NO<sub>2</sub> is near the surface well below the clouds. Second, is the  
195 reduction in the number of measurements during a fixed 20 second measuring period causing a  
196 decrease in the signal to noise ratio. The weather during the campaign was occasionally very cloudy,  
197 which caused some missing NO<sub>2</sub> and O<sub>3</sub> data. However, most of the cloudy days were light to moderate  
198 cloud cover, which permitted C(NO<sub>2</sub>) amounts to be determined, but with lower precision compared to  
199 clear-sky direct sun measurements (e.g., Fig.s 2a and b). When the cloud cover becomes sufficiently  
200 thick, precision is reduced (increased point-to-point scatter) and the spectral fitting error increases. A  
201 small percentage of data points with high retrieval error, C(NO<sub>2</sub> Error) > 0.1 DU, have been removed  
202 from the data set.

203  
204  
205 Figures 3 and 4 summarize all of the Pandora C(NO<sub>2</sub>) data obtained during the KORUS-AQ  
206 campaign. Figure 3 presents histograms in percent frequency of occurrence for all nine sites. All of the  
207 sites located within or downwind of major cities have production of NO<sub>x</sub> mainly from transportation and  
208 power generation as its major sources. The ratio of transportation NO<sub>x</sub> production compared to all  
209 other sources is estimated as up to a factor of three (Kim et al., 2013). Of these sites, Anmyeondo  
210 frequently (40%) retrieves values of C(NO<sub>2</sub>) that are close to the typical stratospheric values of  $0.1 \pm 0.05$   
211 DU. Other sites occasionally have clean days with similar low values.

212  
213

214 The Seoul site frequently has amounts of  $C(NO_2)$  greater than 2 DU. The same is true of Olympic  
215 Park, located in the eastern part of the Seoul metropolitan area. For locations increasingly distant from  
216 Seoul, the amount of  $C(NO_2)$  decreases in response to smaller local emissions, since the short chemical  
217 lifetime of  $NO_2$  normally precludes long distance transport. Compared to Seoul, the two smaller  
218 southern cities, Gwangju and Busan, have relatively low levels of  $C(NO_2)$  on most days, with the most  
219 typical values ranging from 0.3 to 0.5 DU, although high values exceeding 2 DU can occur on rare  
220 occasion.

221  
222 Figure 4 shows the same data as Fig. 3, but in the form of a time series covering the KORUS-AQ  
223 period. The daily variation (at least one point every two minutes) is shown in the vertical extent  
224 corresponding to each day's data. Figures 3 and 4 show that sites near Seoul metropolitan (Olympic  
225 Park) area have larger amounts of pollution compared to those further away (Taehwa, Songchon, and  
226 Yeosu). Even though average  $C(NO_2)$  amounts are much lower at Songchon and Yeosu, there are times  
227 when the pollution levels are quite high ( $C(NO_2) > 2$  DU, Figs. 4 and 5). There are days when the amount  
228 of  $C(NO_2)$  gets close to 4 DU in Seoul, 3 DU in Olympic Park and Busan, and 4 DU for one day in Yeosu  
229 (April 27). The southern cities, Busan and Gwangju are much less polluted on average, which results in a  
230 much smaller effect on adjacent regions. Busan is located on the southeastern coastline, so that some of  
231 its  $NO_2$  pollution dissipates over the ocean, except for occasional days when very high amounts (3 DU)  
232 occur. Anmyeondo is quite clean, since it is located on the western coast well south of Seoul. The most  
233 frequently occurring  $C(NO_2)$  value at Anmyeondo is 0.15 – 0.2 DU, which means that the measured  $NO_2$   
234 amount are partly from the stratosphere ( $0.1 \pm 0.05$  DU) with very little tropospheric or boundary layer  
235  $NO_2$ . There are occasional  $C(NO_2)$  plumes that could be from industrial activity to the north, and,  
236 perhaps, from China. Transport of  $NO_2$  from China occurs episodically in significant amounts (Lee et al.,  
237 2014).

### 238 239 **3 Diurnal Variation of $C(NO_2)$**

240  
241 Grouping the diurnal variation together from multiple days (Fig. 5) reveals a pattern to  $NO_2$   
242 emissions and accumulation related to the main  $NO_2$  emission sources (automobiles and power  
243 generation) for the 3 largest cities in Korea: Seoul (Pan40), Busan (Pan17), and Gwangju (Pan26). For  
244 Seoul, the amounts of  $C(NO_2)$  during the morning (1 DU at 10:00) are much less than later in the  
245 afternoon (over 2 -3 DU at 16:00) on almost every day with values occasionally reaching as high as 6 DU.  
246 Even the relatively low morning values of  $C(NO_2)$  represent a significant amount of pollution. The 6 DU  
247  $C(NO_2)$  amount in Seoul is unusual, but coincides with the peak values frequently occurring in the late  
248 afternoon.  $C(NO_2)$  behavior at nearby Olympic Park to the east of Seoul is very similar to Yonsei  
249 University in the heart of Seoul, even though Olympic Park's traffic density is lower than Seoul. Olympic  
250 Park is close enough to the metropolitan Seoul area for the transport of  $NO_2$  combined with local  
251 production from traffic to produce a very similar diurnal pattern. The moderately large city of Busan also  
252 has high values of  $NO_2$ , occasionally reaching 3 DU in the afternoon. Busan has relatively low values of  
253  $NO_2$  in the morning, having peaks in the mid-afternoon and declining in the late afternoon. Gwangju,  
254 located in the southwest, is a smaller city with less pollution (peak values = 1.6 DU) and does not have as  
255 distinct an afternoon maximum.

256 The panels in Fig. 5 for Taehwa Mtn. and Anmyeondo show regions outside the Seoul  
257 metropolitan area that still show substantial amounts of NO<sub>2</sub>. Compared to Seoul, the Taehwa site is a  
258 semi-rural location with only a small amount of car traffic in the immediate area. However, there are  
259 major highways about 6 km from the site that are close enough to permit transport of NO<sub>2</sub> to the  
260 Taehwa Mountain site. All of the sites showed a tendency to have peak NO<sub>2</sub> occur in the late afternoon.  
261 Anmyeondo on the west central coast of Korea shows C(NO<sub>2</sub>) amounts that are quite low with  
262 occasional plumes arriving from the north or the west (China).

263 The basic daily pattern of C(NO<sub>2</sub>) in urban Korea arises from large amounts of automobile traffic  
264 and power plants emitting NO<sub>x</sub> (for modern automobiles, roughly 99 % NO and 1 % NO<sub>2</sub>). An FTIR  
265 analysis of automobile exhaust shows that NO is emitted at 127 ppm, NO<sub>2</sub> at 1.6 ppm, HCHO at 39 ppm,  
266 and CH<sub>3</sub>OH at 139 ppm as part of the main emissions containing H<sub>2</sub>O (144 ppm) and CO<sub>2</sub> (122 ppm).  
267 (<https://tools.thermofisher.com/content/sfs/brochures/D10248~.pdf>); see also Walters et al., 2015).

268 NO quickly converts into NO<sub>2</sub> in the presence of ozone and volatile organic compounds VOCs in  
269 the atmosphere and can convert back to NO by solar photolysis. KORUS-AQ results frequently show  
270 increasing NO<sub>2</sub> during the day with peaks in the afternoon. For these days the measurements imply that  
271 the amount of locally produced NO<sub>x</sub> and conversion into NO<sub>2</sub> dominates the losses of NO<sub>2</sub> by photolysis  
272 and transport out of the region. Other days occasionally show a different behavior, with NO<sub>2</sub> peaks in  
273 the morning and a decline thereafter suggesting transport out of the region.

#### 274 **4 Longer-Term Changes in C(NO<sub>2</sub>)**

275 Some of the sites used for the KORUS-AQ campaign (Gwangju and Anmyeondo) had PSIs set up  
276 in April 2015, about one year before the start of the campaign. Two other sites (Seoul and Busan) have  
277 PSI C(NO<sub>2</sub>) data starting in 2012. The extended data sets for Seoul and Busan provide the opportunity to  
278 estimate 5-year changes in C(NO<sub>2</sub>) amount and seasonal dependence.

279 In Fig. 6, the daily variation over one year at Gwangju and Anmyeondo are evaluated to estimate  
280 one year secular trends. The vertical extent in the time series is not noise or uncertainty, but rather the  
281 80 second per data point variability throughout each day (e.g., see Fig. 2). Before calculating linear least  
282 squares slopes, the unadjusted time series (grey data points in Panels A and D) were deseasonalized  
283 (grey data points in Panels B and E) by subtracting a function with zero slope derived from a 30 day  
284 running average (dark line in panels A and D or the identical curves in C and F). The running average  
285 curves in panels A and D are shown with expanded scale in panels C and F to clearly show the seasonal  
286 variation. The “zero slope functions” ZM(t) are obtained by subtracting a linear least squares fit L(t) to  
287 monthly running average curves M(t) in panels C and F to form zero slope functions ZM(t) = M(t) – L(t).  
288 The results ZM(t) are functions that look similar to the M(t) plots in panels C and F, but with zero slopes.  
289 The resulting ZM(t) are then subtracted from the respective original time series (grey circles) in panels A  
290 and D. The results are the grey circles in Panels B and E. Similar monthly running means are shown in  
291 Panels B and E that have almost no monthly variations (see appendix Fig. A1).

292 The linear trends in Figs. 6B and 6E suggest that there was an increase in pollution levels in  
293 Gwangju and Anmeondo over the period of observation. The southern city of Gwangju (Pan 26) has



294 higher average C(NO<sub>2</sub>) amounts, 0.34±0.19 DU, compared to the relatively clean coastal site  
295 Amnyeondo, 0.26±0.14 DU. Gwangju seasonal cycle has a minimum in C(NO<sub>2</sub>) amount in September-  
296 October and a very broad maximum from December to May. The Gwangju PSI is located away from  
297 major city traffic on a university campus (Gwangju Institute of Science and Technology, GIST) so that the  
298 average amount of NO<sub>2</sub> (about 0.34 DU) is moderate with some days reaching 1.5 DU. The slopes are  
299 statistically significant at the 2-standard deviation level ( $p < 0.05$ ) and imply that C(NO<sub>2</sub>) was increasing  
300 at a substantial rate. However, the period of observation was too short to estimate multi-year long-term  
301 trends. Additional long-term monitoring of these sites would be desirable for air quality purposes.

302 The PSI on Amnyeondo was located away from a commercial area with moderate traffic and  
303 very near the shore of the Yellow Sea at a regional Global Atmosphere Watch (GAW) station. For  
304 Amnyeondo there is a clear seasonal cycle similar to that in Gwangju with a minimum in September-  
305 October and a broad maximum during the winter-spring months. Amnyeondo had an average amount  
306 of 0.25 DU, which is lower than observed at Gwangju.

307  
308 Figures 7 and 8 each contain an approximately 5-year daily time series (grey) for Seoul (Yonsei  
309 University) and Busan (Pusan University) and a linear fit to a deseasonalized version of the time series.  
310 Since the observations at both sites had an extended period of missing data, the slopes were estimated  
311 separately for each segment and for the combined time series. Both Seoul and Busan show a steady  
312 reduction in NO<sub>2</sub> air pollution with an average reduction of about -4 % per year. A recent paper by  
313 Duncan et al., (2016) estimated a decrease in C(NO<sub>2</sub>) for Seoul in about a 10 x 10 km box of about 1.6 ±  
314 1.4 % per year over the 2004 to 2013 period based on a 2014 average C(NO<sub>2</sub>) amount of 0.6 DU, or  
315 about half of the average value 1.3 ± 0.8 DU observed by the PSI. The larger reduction in C(NO<sub>2</sub>)  
316 measured by the PSI is caused by a reduction in higher than average afternoon C(NO<sub>2</sub>) amounts that are  
317 rarely observed by OMI overpass at 13:30 local time. OMI is a polar orbiting push broom hyperspectral  
318 instrument (300 – 500 nm with resolution of 0.45 nm in the UV and 1 nm in the visible and a spatial  
319 resolution of 13 x 24 km<sup>2</sup>) onboard the AURA satellite. The high observed late afternoon values are not  
320 restricted to Seoul, but occur for all of the urban areas where the PSI has been deployed. The high late  
321 afternoon values do not regularly occur in remote rural areas such as Amnyeondo.

322 Seoul and Busan C(NO<sub>2</sub>) measurements are remarkable for the large peak amounts that are seen  
323 on most days compared to the 1.5 to 2 DU peak values for Gwangju and Amnyeondo. For Yonsei, the  
324 peak values range above 5 to 6 DU in the years 2012 to 2015, but decrease somewhat in 2015 to 2016.  
325 In 2015 - 2016, the decrease appears to be large, but is only 0.2 DU relative to a mean of about 1.2 DU.  
326 A smaller decrease appears for Busan (Fig. 8) relative to a mean of about 0.6 DU. All of the PSI  
327 measurements show very high values of NO<sub>2</sub> during almost every day when measurements were  
328 possible. Since the NO<sub>2</sub> concentrations represented by these large column amounts are probably in the  
329 boundary layer near the sources of NO<sub>2</sub>, there is a strong effect on local air quality.

330  
331  
332  
333

## 334 5 Comparison with OMI Satellite Overpass Data

335  
336 Seoul and Busan have 5-year PSI data records (Figs. 9a and 9b), and Gwangju has a 1-year data  
337 record (Figs. 6 and 10) spanning the KORUS-AQ campaign. The PSI  $C(NO_2)$  can be matched in time ( $\pm 8$   
338 minutes) with the overpass time from OMI (Ozone Monitoring Instrument) onboard the AURA satellite  
339 (mid-day overpass times  $13:30 \pm 90$  minutes). Figure 9a shows the  $C(NO_2)$  daily variation at the OMI  
340 overpass time with far more high values of  $C(NO_2)$  from the PSI than observed by OMI. The solid lines  
341 represent the seasonal dependence, which are shown separately in Fig. 9b along with the  $C(NO_2)$   
342 differences, PSI - OMI. The result is that the average PSI values are double those observed by OMI's  
343 large FOV. (OMI Version 03: <https://avdc.gsfc.nasa.gov/index.php?site=666843934&id=13>)  
344

345 The seasonal dependence (Fig. 9b) of  $C(NO_2)$  from OMI for both Seoul and Busan is fairly  
346 regular, with maxima in January of each year and minima in July-August. The seasonal behavior of  
347  $C(NO_2)$  obtained from the PSI for Seoul varies with high values extending from January into the summer  
348 months and with minima varying from August in 2012, September-October in 2013, missing in 2014, July  
349 in 2015, and June in 2016. For Busan, the maxima occur in the Spring for 2013 and 2014, October for  
350 2015, and in the Spring for 2016. The minima are also variable. The difference between OMI and PSI  
351 retrievals depends on local conditions for PSI and on an area average for OMI.  
352

353 Figure 9b shows that the PSI has a mean difference compared to OMI in Busan of 0.35 DU and  
354 peak values (up to 2.5 DU at 13:30 and 4 DU in the late afternoon). The differences are important when  
355 considering pollution effects on human health (Krafta et al., 2005; Latza et al., 2009). Even larger  
356 differences are observed in Seoul, where the mean difference is 0.58 DU between Pandora and OMI at  
357 the satellite overpass time. The results from PSI suggest that local ground-based monitoring of pollution  
358 is important for estimating their impact on human health, particularly since amounts of  $C(NO_2)$   
359 occurring later in the afternoon exceed the amounts at the time of the satellite overpass.  
360

361 A comparison with Lowess(0.1) fits (Locally Weighted least squares fit to 0.1 of the data points,  
362 (Cleveland, 1981)) to the matched Pandora vs OMI overpass data (about 3-month averages) shows that  
363 PSI  $C(NO_2)$  is larger than OMI measured  $C(NO_2)$  mostly because of its much smaller  $2^\circ$  field of view (a  
364 circle of 35 meters diameter at 1 km altitude) compared to OMI's FOV of  $13 \times 24 \text{ km}^2$  at nadir, which  
365 may encompass areas outside of the city or the adjacent ocean areas. For example, the center of Seoul  
366 is about 48 km from the Yellow Sea, while the OMI overpass file lists FOV center distances of over 60 km  
367 from Seoul. Another possible reason for the differences is that OMI  $C(NO_2)$  retrievals use  $NO_2$  vertical  
368 profile shape factors from the low resolution ( $\sim 110 \times 110 \text{ km}$ ) Global Model Initiative (GMI) model  
369 simulation to calculate air mass factors that are used to determine observed tropospheric  $NO_2$  vertical  
370 columns, while much finer resolution profiles are needed to more accurately represent highly polluted  
371 urban areas such as Seoul. Increases in OMI retrieved tropospheric column  $NO_2$  up to 160 % are found  
372 when using model derived  $1.33 \times 1.33 \text{ km}^2$  profile shape factors (Goldberg et al., 2017). The effect of  
373 moderate amounts of cloud or aerosol have little effect on the PSI direct-sun spectral fitting retrieval of  
374  $C(NO_2)$  as shown in Fig. 2. OMI and MAXDOAS retrievals are sensitive to the presence of aerosols and

375 clouds (Kanaya et al., 2014), which may contribute to the underestimate of C(NO<sub>2</sub>) by OMI even after  
376 corrections are made for retrieved aerosol and cloud amounts (Chimot, et al. 2016).

377  
378 The implications for assessing clean air indices suggest that OMI underestimates the human  
379 health effect from trace gases such as NO<sub>2</sub>, especially in highly populated urban areas. Figure 5 gives a  
380 much clearer picture of the degree of pollution than is possible with just the 13:30 OMI comparison  
381 measurements, since the late afternoon is the time of maximum pollution.

382  
383 The city of Gwangju is much smaller than Busan, with less industrial activity, especially  
384 automobiles. PSI observations at GIST show much closer agreement with OMI (Fig. 10), especially since  
385 GIST is located within the city boundaries, but in an area with much less concentrated industrial activity  
386 compared to the center of Gwangju. The large OMI FOV over a relatively clean area reduce the OMI  
387 difference in measured NO<sub>2</sub> amount compared to the PSI C(NO<sub>2</sub>) amounts. OMI still measures less than  
388 the PSI ( $0.12 \pm 0.15$  DU), but the mean difference is not statistically significant. However, OMI clearly  
389 misses the high values of C(NO<sub>2</sub>) that are present in the PSI observations.

390  
391

## 392 **5.1 Comparison with 4STAR DC-8 Overpass Data**

393  
394 C(NO<sub>2</sub>) results were obtained by the Spectrometer for Sun-tracking Sky-Scanning Atmospheric  
395 Research (4STAR) flown on-board the DC-8 during KORUS-AQ and compared with the PSI (Fig. 11). The  
396 4STAR is an airborne sunphotometer, capable of measuring total C(NO<sub>2</sub>), C(O<sub>3</sub>), water vapor and AOD  
397 columns in its direct-sun mode (Segal-Rozenhaimer et al., 2014; Shinozuka et al., 2013), which is similar  
398 to the mode used by the PSI network.

399  
400 A detailed description of 4STAR is given in Dunagan et al., (2013). In brief, the instrument has  
401 two structurally rigid grating array spectrometers that are combined to yield continuous spectra  
402 between 300-1700 nm. The instrument sampling rate is 1 Hz, and the nominal integration time used for  
403 C(NO<sub>2</sub>) retrievals is 50 ms (with six spectra averaged per one sampling period). Dark counts are  
404 measured every 20 min using a shutter mechanism. The 4STAR light collection system has fiber optic  
405 bundle foreoptics that is connected to the spectrometers. A two-axis motion control system with analog  
406 feedback provides active tracking of the solar disk. The instrument full field of view (FOV) is ~1.25°.   
407 C(NO<sub>2</sub>) is retrieved following a method described in Segal-Rozenhaimer et al. (2014), but using the 460-  
408 490 nm spectral range. A series of 4STAR columnar NO<sub>2</sub> values above aircraft (for legs below 300 m)  
409 taken from DC8 “missed approach” maneuvers overflying Olympic Park PSI station, within a radius of 5  
410 km, are shown in Fig. 11. There is a relatively good correlation ( $R^2=0.7$ ), with a slight positive bias of  
411 4STAR compared with the PSI values. This might result from higher noise effects (i.e. small amount of  
412 spectra averages) for 4STAR during the fast change of altitude when the aircraft performs its “missed  
413 approach” overpasses over the PSI stations. Relaxing the altitude constraint to include legs below 500 m  
414 showed good agreement with the PSI station at Taewha Mountain, but with an overall lower correlation  
415 coefficient ( $R^2=0.54$ ), which is expected due to averaging of larger vertical range. As with PSI, 4STAR  
416 shows better agreement with OMI C(NO<sub>2</sub>) for low values of C(NO<sub>2</sub>), but considerable differences over

417 polluted areas (Segal-Rozenhaimer et al., *in prep.*), when 4STAR C(NO<sub>2</sub>) values are averaged within each  
418 of the OMI pixels corresponding to the flight path for each of the days.

419

## 420 **6 Formaldehyde from Five Korus-AQ Sites**

421

422 PSI makes two sets of direct-sun measurements every 80 seconds. One set is for measurements  
423 in the visible range (380 – 525 nm used for NO<sub>2</sub>) and the other is for the UV range (290 – 380 nm with a  
424 filter, U340, which blocks visible light). Formaldehyde is derived from the same set of spectral  
425 measurements used for ozone (i.e., with a U340 blocking filter), but using the spectral range 332 - 359  
426 nm. Sources of error in the C(HCHO) retrieval arise from the selection of the fitting window and the  
427 amount of C(HCHO) remaining in the reference spectrum after application of the modified Langley  
428 estimation (MLE) method of calibration (Herman et al., 2009, Spinei et al., 2018). The MLE extrapolation  
429 to zero C(HCHO) could have an offset error of 0.1 to 0.2 DU. Selecting different fitting windows can also  
430 cause the C(HCHO) retrievals to differ. For example, a wider alternate fitting window, 324 -360 nm,  
431 retrieves HCHO values that are about 8 % higher because of different amounts of interference from  
432 overlapping absorption by O<sub>3</sub>, NO<sub>2</sub>, and BrO at the spectral resolution of 0.5 to 0.6 nm currently in use.  
433 Absolute offset errors do not affect the retrieval precision (relative column amounts), which is  
434 approximately 0.1 DU. A detailed analysis of the algorithms and uncertainties is discussed by Spinei et  
435 al., 2018.

436

437 The Olympic Park area has much more vegetation than central Seoul for the production of  
438 isoprene (<http://www.olympicpark.co.kr>), which is a significant source of the chemicals needed for  
439 formaldehyde production in the atmosphere (Luecken et al., 2012). Observations from PSI show that  
440 C(HCHO) starts out every day at low levels 0.6 DU at about 08:00 and increases to over 2 DU until 18:00  
441 (Figs 12 and 13). Most HCHO arises from photochemical production, while a significant fraction is  
442 chemically derived from automotive emissions in densely populated urban areas (Friedfeld et al., 2002;  
443 Garcia et al., 2006; Lei et al., 2009; Liteplo et al., 2010). Regardless of the precursor source, HCHO forms  
444 in the atmosphere primarily by photochemistry, which causes HCHO to usually be a minimum early in  
445 the day, increase into the afternoon, and decline towards evening. The PSI C(HCHO) observations (Figs.  
446 12 and 13) support this pattern of daily variation.

447

448

449 A summary of the daily time dependence of C(HCHO) at Olympic Park during the entire  
450 KORUS-AQ campaign is shown in Fig. 13. As in Fig. 12, minimum values are observed in the  
451 morning (06:00 – 08:00) before the chemical and direct sources of HCHO are significant. There  
452 is strong buildup during the day that reached a maximum between 15:00 to 16:00, and then  
453 diminished towards sunset. As with NO<sub>2</sub>, the daily pattern of late afternoon peaking of HCHO  
454 amounts presents a problem for polar orbiting satellite observations (e.g., OMI observations at  
455 13:30) assessing air quality.

456

457

458  
459  
460  
461  
462  
463  
464  
465  
466  
467  
468  
469  
470  
471  
472  
473  
474  
475  
476  
477  
478  
479  
480  
481  
482  
483  
484  
485  
486  
487  
488  
489  
490  
491  
492  
493  
494  
495

Figure 14 shows two altitude profiles acquired by the Compact Atmospheric Multispecies Spectrometer (CAMS) (Richter et al., 2015) onboard the DC-8 aircraft as it spiraled over the Olympic Park area on 4 May 2016 in the morning and at midday. Quoting from Richter et al., (2015), “CAMS is a multi-species spectrometer configured for the simultaneous detection of ethane (C<sub>2</sub>H<sub>6</sub>) and formaldehyde (CH<sub>2</sub>O). The spectrometer utilizes a tunable, fiber optically pumped difference frequency generation laser source in combination with a Herriott type multi-pass absorption cell with an effective path length of 89.6 m”

The morning integrated amount on 4 May was  $1.02 \times 10^{16}$  molecules  $\text{cm}^{-2}$  (0.38 DU) and the afternoon amount was  $6.95 \times 10^{15}$  molecules  $\text{cm}^{-2}$  (0.26 DU), both substantially less than the PSI measured values of 0.48 DU and 0.42 DU, respectively. There were no surface measurements of HCHO mixing ratio on 4 May at Olympic Park. On 2 June at 11:40 there was a surface measurement 3.94 ppb. Including the surface measurement in the profile integral yields  $\text{Integ}(0.026, 7.2 \text{ km}) = 0.55 \text{ DU}$ , while PSI measured 1.2 DU, which is consistent with the differences shown in Fig. 14. The notation in Fig 14 is

$$\text{Integ}(z_1, z_2) = \int_{z_1}^{z_2} \text{HCHO}(z) dz \text{ for the altitudes } z_1 \text{ to } z_2, \text{ where } z \text{ is in km.}$$

The profiles used data for lower altitudes obtained from aircraft “missed approach” maneuvers at a nearby Seoul Airbase, 8.5 km from Olympic Park, (Fig. 15). When available, a single surface altitude point was added using ground-based volume mixing ratio measurements obtained from US Environmental Protection Agency measurements using quantum cascade laser instruments (Hottle et al., 2009, Spinei et al., 2018 and references therein). The DC-8 minimum altitude exactly over Olympic Park was typically around 0.4 km above the surface (black circles Fig. 15). Large vertical DC-8 HCHO gradients were observed as the DC8 descended to lower altitudes over Seoul Airbase. A comparison of 10-second DC-8 HCHO averages at the points of closest spatial approach to the Olympic Park (black circles) site on June 4, for example, to peak HCHO measurements during missed approaches at the nearby Seoul Airbase (20 – 40 meters above the ground) revealed ratios in the observed HCHO (black circles) ranging between 75 % to 83 % of the maximum values near the surface. Since Olympic Park DC-8 overpasses miss significant near surface HCHO amounts, the profiles shown in Figs. 14 and 16 incorporate the HCHO amounts down to the surface at an altitude of 0.026 km asl derived from the “missed approach” at Seoul airbase. HCHO measurements above the maximum altitude over Olympic Park (see Fig. 14 and 16) were taken from the closest time over the Taewha Mtn. site, 28 km from Olympic Park. The assumption is that the horizontal gradients above 2.2 km (Fig. 15) can be neglected,

496 After conversion from mixing ratio to molecules/cm<sup>3</sup> using the measured atmospheric  
497 density, the resulting profile data were integrated from the minimum (0.026 km asl, Table 1) to  
498 the maximum heights indicated in Fig. 14. The result is 0.38 DU at 07:54 and 0.26 DU at 11:54  
499 compared to the measurements from the Pandora instrument 0.48 and 0.38 DU. The derived  
500 vertical HCHO columns from the DC8 data in Fig. 14 A and B are 79 % of PSI measured C(HCHO) in the  
501 morning and 68 % of PSI C(HCHO) at midday (Fig 14 C).

502  
503 A similar comparison is shown in Fig. 16 for 5 June 2016 where the amount of C(HCHO)  
504 is much larger than on 4 May. Integration of the measured profiles yields column densities of  
505 0.60 and 0.82 DU at 08:30 and 15:21 hours. For this case, at both times the DC8 values are  
506 about 77 % and 63 % of the PSI measured column amounts, 0.78 and 1.3 DU. For both cases in  
507 Figs. 14 and 15 the 23 % to 37 % differences are outside of the expected error from PSI fitting  
508 window selection and from residual HCHO included in the MLE calibration method.

509  
510 Another Olympic Park case on 9 June 2016 shows DC8=0.79 vs PSI=1 DU at 08:06,  
511 DC8=0.74 vs PSI=1.3 DU at 12:12, and DC8=1.13 vs PSI=1.9DU, or the DC8 measurements are 79  
512 % and 57 % less than the PSI total column HCHO. All of the remaining comparisons of DC8  
513 profile results with PSI C(HCHO) show similar results. The reasons for the disagreement between  
514 C(HCHO) measured by direct sun observations (PSI) and the integrated column density from aircraft  
515 measurements of HCHO VMR are not known. Contributions to the differences include the selection of  
516 the PSI wavelength window (332 - 359 nm) and possible interference from overlapping NO<sub>2</sub> and O<sub>3</sub>  
517 absorption that are not properly included, and, more likely, the use of CAMS measured volume mixing  
518 ratios at the lowest altitudes from the nearby Seoul airbase, 8.5 km from Olympic Park, where spatial  
519 variation may affect the calculation of C(HCHO). The use of Taehwa Mtn. data for higher altitudes over  
520 Olympic Park contributes 25 % for 3 of the above cases and 50 % for 4 May 2016 at 07:54 (Fig.  
521 14A). This is probably not the reason for the disagreement between CAMS and PSI, since the percent  
522 underestimate for CAMS over Taehwa is about the same magnitude (Table 2) as over Olympic Park.

523  
524 PSI measurements show that Olympic Park produces more HCHO almost every day than  
525 observed at the Yonsei University in Seoul and Taehwa Mountain sites (Figs. 12, 17, 18). The  
526 hourly variations observed during the KORUS-AQ campaign at the Yonsei University in Seoul  
527 and at Taehwa Mountain sites are similar to Olympic Park even though most of the HCHO is  
528 locally produced by photochemistry, but has a relatively short lifetime of a few hours in  
529 polluted air where there is significant ozone and OH. However, at typical wind speeds of 10 -20  
530 km/hour and a chemical lifetime of 2.5 hours (Dufour et al., 2009), HCHO can be transported  
531 about 25 – 50 km, which is far enough for some transport of HCHO between the PSI sites at  
532 Yonsei, Olympic Park, and Taehwa Mtn. DC8 CAMS results over the Taehwa Mtn. site compared  
533 to PSI are given in Table 2 with differences similar to Olympic Park

534

535

Table 2 Taehwa Mtn DC8 compared to PSI measurements (see 10 Jun in Fig. 18)

Date	LT	DC8 HCHO DU	PSI HCHO (DU)	Percent
11 May	08:25:19	0.4	0.6	67
18 May	08:34:26	0.4	0.5	80
30 May	12:05:00	0.5	0.9	56
10 Jun	08:22:45	1	1.16	86
10 Jun	12:22:53	1	1.5	67
10 Jun	15:46:03	1	1.3	77

536

537

538 Figure 19a and 19b summarizes all of the C(HCHO) data obtained during KORUS-AQ at  
539 the five sites. The graphs on the left show all of the data points (light gray circles) as a function  
540 of the local time and a Lowess(0.1) fit to the data showing the average hourly behavior. The  
541 spread of the data about the Lowess(0.1) fit represents the day-to-day variation at a given local  
542 time. On average, Mt. Taehwa tends to increase throughout each day, while Yonsei and  
543 Olympic Park show maxima at 14:00 and 15:30, respectively. Similarly, in Fig. 18b Yeogju  
544 increases during the day having a maximum at 17:42 while Amnyeondo has a broad peak with  
545 maxima at 12:00 and 13:42.

546

547 The histograms on the right side of Fig. 19 represent the percent frequency of  
548 occurrence of C(HCHO) in 0.1 DU bins. C(HCHO) at Mt. Taehwa and Seoul rarely exceeds 1.5 DU  
549 compared to Olympic Park where C(HCHO) > 2 DU for a significant fraction of time. The most  
550 frequent values are 0.6 DU for Seoul, 0.9 DU for Mt Taehwa, and over 1 DU for Olympic Park.  
551 Olympic Park also has a broader distribution towards higher values of C(HCHO) than other sites.

552

553 The general intra-day C(HCHO) time dependence and C(HCHO) percent occurrence are  
554 shown for two additional sites (Fig. 19b), Yeogju and Amnyeondo. Yeogju shows an increase in  
555 C(HCHO) from morning to a peak value of 0.85 DU at 14:42, which then declines after 16:00. In  
556 contrast, Amnyeondo is almost symmetric with the sun position, having a maximum of about  
557 0.77 DU near 12:00 and 13:42 hours.

558 The average change in C(HCHO) during the spring campaign at the five sites is  
559 summarized in Fig. 20. Of the sites, Olympic Park showed the largest change rate, 58 %/Month  
560 followed by Amnyeondo at 50 %/Month, then Taehwa (33 %/Month), Yonsei Seoul (25  
561 %/Month), and Yeogju (-13 %/Month). Amnyeondo tends to have lower C(HCHO) amounts  
562 because of its relatively isolated coastal location. These 2-month trends include seasonal  
563 increases during the campaign months May and June, 2016.

564 It is difficult to compare PSI C(HCHO) with OMI for the KORUS-AQ period, since OMI  
565 overpass C(HCHO) data for 2016 have some missing days (Fig. 21). For days with matching  
566 data points over Seoul, PSI C(HCHO) (approximately 0.8 DU) is almost always larger than the  
567 OMI values (0.2 DU) plus a few very high PSI values and two high OMI values. The general  
568 day-to-day variations are similar.

569

## 570 **7 Summary**

571

572 Nine Pandora Spectrometer Instruments, PSI, were installed at 8 sites in South Korea as part of  
573 the KORUS-AQ ground, aircraft, and satellite measurements for air-quality studies. The measurements  
574 made during the months of April to June by PSI showed that are very high amounts of urban pollution  
575 from NO<sub>2</sub> and HCHO, and more moderate, but still high values in Mt Taewha and Yeogju, which are  
576 some distance from the major urban centers,. An exceptional location was Amnyeondo, which is located  
577 on a west-coastal island adjacent to the Yellow Sea about 100 km south of Seoul. The urban areas show  
578 minimum values in the morning that rise rapidly throughout the day, peaking in the late afternoon for  
579 both C(NO<sub>2</sub>) and C(HCHO).

580

581 PSI direct-sun retrieved values of C(NO<sub>2</sub>) and C(HCHO) are always larger than OMI retrieved  
582 C(NO<sub>2</sub>) and C(HCHO) for the OMI overpass times ( $13.5 \pm 0.5$  hours). In urban areas, PSI C(NO<sub>2</sub>) averages  
583 are at least a factor of two larger than OMI averages. Similar differences are seen for C(HCHO) in Seoul.  
584 However, late afternoon values measured by PSI are even larger, implying that OMI measurements  
585 underestimate the effect of poor air quality on human health. The primary cause of the OMI  
586 underestimate is the large OMI FOV that includes regions containing low values of pollutants. In  
587 relatively clean areas, PSI and OMI are more closely in agreement.

588

589 PSI retrieved C(NO<sub>2</sub>) amounts for Seoul frequently exceed 2 DU and occasionally reach 6 DU.  
590 Other urban centers in the south, Busan and Gwangju, have smaller C(NO<sub>2</sub>) amounts, but exhibit a  
591 similar strong diurnal pattern, namely low values in the morning and high values later during midday.  
592 This behavior is expected because of the large number of urban automobiles and concentrated industry.  
593 Urban areas downwind from Seoul show high C(NO<sub>2</sub>) amounts, but also show daily minimum amounts in  
594 the morning that increase later in the day. Two of the sites, Seoul and Busan, have long-term C(NO<sub>2</sub>)  
595 data records, 2012 – 2016, that suggest a gradual decrease in C(NO<sub>2</sub>) amounts in Korea. When  
596 compared with OMI, both ground-based PSI's and the 4STAR aircraft instrument onboard the DC8 show  
597 that the correlation is best for small values of C(NO<sub>2</sub>), most often seen in the troposphere and  
598 stratosphere and worst for high values that are usually in the boundary layer near their local sources. In  
599 Olympic Park, the measurements of significant values of C(HCHO) and high values of C(NO<sub>2</sub>) in the  
600 afternoon suggest that there are increased boundary layer amounts of ozone.

601

602 C(HCHO) amounts were obtained for five sites, Yonsei University in Seoul, Olympic Park, Taehwa  
603 Mtn., Amnyeondo, and Yeoju. Of these the largest amounts of C(HCHO) were observed at Olympic Park,



604 and Taehwa Mountain, both surrounded by significant amounts of vegetation. Comparisons of PSI  
605 results were made with overflights on the DC8 aircraft for Taehwa Mtn and Olympic Park showing a  
606 significant difference in total column HCHO. In all cases, PSI measured substantially more C(HCHO) than  
607 obtained from integrating the altitude profiles measured from the DC8 overflights.  
608

## 609 Appendix

610  
611 Figure A1 illustrates the deseasonalization of the time series in Fig.6. The left panel reproduces  
612 the solid black curve in Fig. 6A or 6C in the inset. The right panel reproduces the solid curve in Fig. 6B  
613 and is magnified in the inset. The seasonal dependence in the left panel inset is almost non-existent in  
614 the right panel inset  
615

616

617

618

## 618 Data Sources

619 OMI Formaldehyde HCHO Version 03: <https://avdc.gsfc.nasa.gov/index.php?site=1113974256&id=81>

620 OMI Nitrogen Dioxide NO<sub>2</sub> Version 03 <https://avdc.gsfc.nasa.gov/index.php?site=666843934&id=13>

621 Pandora KORUS-AQ <https://avdc.gsfc.nasa.gov/pub/DSCOVER/Pandora/DATA/KORUS-AQ/>

622

623 **Author Contributions**

624

625 Jay Herman: Wrote most of the paper and performed the analysis and comparisons with the DC-8  
626 aircraft measurements

627 Elena Spinei: Derived the formaldehyde altitude profiles suitable for comparison with Pandora data

628 Alan Fried: Obtained the HCHO profile data from the DC-8 CAMS instrument

629 Jhoon Kim: Provided support for the installation of Pandora instruments in Korea.

630 Jae Kim: Provided support for the Pandora located in Busan .

631 Woogyung Kim: Provided support in installing the Pandoras and analyzing the raw data

632 Alexander Cede: Provided calibration and data analysis support

633 Nader Abuhassan: Provided Pandora setup in Korea and provided the maintenance of calibration

634 Michal Segal-Rozenhaimer: Provided the 4STAR NO<sub>2</sub> data from the DC-8 flights and the comparison with  
635 Pandora

636

637 The authors declare that they have no conflict of interest.

638 **8 References**

- 639 Boersma, K. F., D. J. Jacob, M. Trainic, Y. Rudich, I. DeSmedt, R. Dirksen, and H. J. Eskes, Validation of  
640 urban NO<sub>2</sub> concentrations and their diurnal and seasonal variations observed from the SCIAMACHY and  
641 OMI sensors using in situ surface measurements in Israeli cities, *Atmos. Chem. Phys.*, 9, 3867–3879,  
642 2009.
- 643 Bernhard, G., C. R. Booth, and J. C. Eshamjian. Version 2 data of the National Science Foundation’s  
644 ultraviolet radiation monitoring network: South Pole. *Journal of Geophysical Research (Atmospheres)*,  
645 109(D21), 2004
- 646 Cede, Alexander, Manual for Blick Software Suite1.3 Version 7, 20 Apr 2017  
647 [https://avdc.gsfc.nasa.gov/pub/DSCOVR/Pandora/Documents/BlickSoftwareSuite\\_Manual\\_v7.pdf](https://avdc.gsfc.nasa.gov/pub/DSCOVR/Pandora/Documents/BlickSoftwareSuite_Manual_v7.pdf)
- 648 Chimot, J., Vlemmix, T., Veefkind, J. P., de Haan, J. F., and Levelt, P. F.: Impact of aerosols on the OMI  
649 tropospheric NO<sub>2</sub> retrievals over industrialized regions: how accurate is the aerosol correction of cloud-  
650 free scenes via a simple cloud model?, *Atmos. Meas. Tech.*, 9, 359-382, [https://doi.org/10.5194/amt-9-](https://doi.org/10.5194/amt-9-359-2016)  
651 359-2016, 2016.
- 652 Cleveland, William S., LOWESS: A program for smoothing scatterplots by robust locally weighted  
653 regression. *The American Statistician*. 35 (1): 54. [JSTOR 2683591](https://www.jstor.org/stable/2683591). [doi:10.2307/2683591](https://doi.org/10.2307/2683591), 1981.  
654
- 655 Dufour, G., F. Wittrock, M. Camredon, M. Beekmann, A. Richter, B. Aumont, and J. P. Burrows,  
656 SCIAMACHY formaldehyde observations: constraint for isoprene emission estimates over Europe?,  
657 *Atmos. Chem. Phys.*, 9, 1647–1664, 2009  
658
- 659 Dunagan, S. E., R. Johnson, J. Zavaleta, P. B. Russell, B. Schmid, C. Flynn, J. Redemann, Y. Shinzuka, J.  
660 Livingston, and M. Segal-Rosenhaimer, 4STAR spectrometer for sky-scanning Sun-tracking atmospheric  
661 research: Instrument technology, *Remote Sens. (Special Issue*  
662 "Optical Remote Sensing of the Atmosphere"), 5, 3872–3895, [doi:10.3390/rs5083872](https://doi.org/10.3390/rs5083872), 2013.
- 663 Fried, A., Walega, J. G., Olson, J. R., Crawford, J. H., Chen, G., Weibring, P., ... Millet, D. B. (2008).  
664 Formaldehyde over North America and the North Atlantic during the summer 2004 INTEX campaign:  
665 Methods, observed distributions, and measurement-model comparisons. *Journal of Geophysical*  
666 *Research*, 113(D10). <https://doi.org/10.1029/2007JD009185>, 2008.
- 667 Friedfeld, S., M. Fraser, K. Ensor, S. Tribble, D. Rehle, D. Leleux, F. Tittel Statistical analysis of primary and  
668 secondary atmospheric formaldehyde, *Atmospheric Environment*, 36, 4767-4775, 2002.
- 669 Garcia, A.R., R. Volkamer, L.T. Molina, M.J. Molina, J. Samuelson, J. Mellqvist, B. Galle, S.C. Herndon, C.E.  
670 Kolb, Separation of emitted and photochemical formaldehyde in Mexico City using a statistical analysis  
671 and a new pair of gas-phase tracers *Atmospheric Chemistry Physics*, 6, 4545-4557, 2006.
- 672 Goldberg D. et al., (2017), A High-Resolution And Observationally Constrained Omi NO<sub>2</sub> Satellite  
673 Retrieval, *Atmos. Chem. Phys. Discuss.*, [doi:10.5194/acp-2017-219](https://doi.org/10.5194/acp-2017-219), 2017.

674 Gueymard, Christian A., The sun's total and spectral irradiance for solar energy applications and solar  
675 radiation models. *Solar energy*, 76(4):423–453, 2004.

676 Herman, Jay, Alexander Cede, Elena Spinei, George Mount, Maria Tzortziou, Nader Abuhassan, NO<sub>2</sub>  
677 Column Amounts from Ground-based Pandora and MFDOAS Spectrometers using the Direct-Sun DOAS  
678 Technique: Intercomparisons and Application to OMI Validation, *J. Geophys. Res.*, 114, D13307,  
679 doi:10.1029/2009JD011848, 2009.

680 Jung, Jinsang, JaeYong Lee, ByungMoon Kim, SangHyub Oh, Seasonal variations in the NO<sub>2</sub> artifact from  
681 chemiluminescence measurements with a molybdenum converter at a suburban site in Korea  
682 (downwind of the Asian continental outflow) during 2015 - 2016, *Atmospheric Environment* 165, 290-  
683 300, 2017.

684 Kanaya, Y., Irie, H., Takashima, H., Iwabuchi, H., Akimoto, H., Sudo, K., Gu, M., Chong, J., Kim, Y. J., Lee,  
685 H., Li, A., Si, F., Xu, J., Xie, P.-H., Liu, W.-Q., Dzhola, A., Postlyakov, O., Ivanov, V., Grechko, E.,  
686 Terpugova, S., and Panchenko, M.: Long-term MAX-DOAS network observations of NO<sub>2</sub> in Russia and  
687 Asia (MADRAS) during the period 2007–2012: instrumentation, elucidation of climatology, and  
688 comparisons with OMI satellite observations and global model simulations, *Atmos. Chem. Phys.*, 14,  
689 7909-7927, <https://doi.org/10.5194/acp-14-7909-2014>, 2014.

690 Kim, Na Kyung, Yong Pyo Kim, Yu Morino, Jun-ichi Kurokawa, Toshimasa Ohara, Verification of NO<sub>x</sub>  
691 emission inventory over South Korea using sectoral activity data and satellite observation of NO<sub>2</sub> vertical  
692 column densities, *Atmospheric Environment* , 77, 496-508, 2013.

693 Kim, Daewon, Hanlim Lee, Hyunkee Hong, Wonei Choi, Yun Gon Lee and Junsung Park, Estimation of  
694 Surface NO<sub>2</sub> Volume Mixing Ratio in Four Metropolitan Cities in Korea Using Multiple Regression Models  
695 with OMI and AIRS Data, *Remote Sens.* 2017, 9, 627; doi:10.3390/rs9060627, 2017.

696 Krafta, Martin, Thomas Eikmannb, Andreas Kapposc, Nino Künzlid, Regula Rappe, Klaus Schneiderf,  
697 Heike Seitzb, Jens-Uwe Voss, H.-Erich Wichmannh, The German view: Effects of nitrogen dioxide on  
698 human health – derivation of health-related short-term and long-term values, *International Journal of*  
699 *Hygiene and Environmental Health*, 208, 305–318, 2005.

700 Kramer, L.J., R. J. Leigh, J. J. Remedios, et al., “Comparison of OMI and Ground-Based in situ and  
701 MAXDOAS Measurements of Tropospheric Nitrogen Dioxide in An Urban Area,” *J. Geophys. Res.* **113**,  
702 D16S39, 2008.

703 Kurucz. Robert L ., New atlases for solar flux, irradiance, central intensity, and limb intensity. *Memorie*  
704 *della Societa Astronomica Italiana Supplementi*, 8:189, 2005.

705 Latza, Ute, , Silke Gerdes, and Xaver Baur, Effects of nitrogen dioxide on human health: Systematic review  
706 of experimental and epidemiological studies conducted between 2002 and 2006, *International Journal*  
707 *of Hygiene and Environmental Health* 212, Pages 271 - 287, [doi.org/10.1016/j.ijheh.2008.06.003](https://doi.org/10.1016/j.ijheh.2008.06.003), 2009.

708 Lee, Greem, Hye-Ryun Oh, Chang-Hoi Ho, Jinwon Kim, Chang-Keun Song, Lim-Seok Chang, Jae-Bum Lee,  
709 Seungmin Lee, Airborne Measurements of High Pollutant Concentration Events in the Free Troposphere  
710 over the West Coast of South Korea between 1997 and 2011, *Aerosol and Air Quality Research*, 16,  
711 1118–1130, 2016.

712 Lei, W., Zavala, M., de Foy, B., Volkamer, R., Molina, M. J., and Molina, L. T.: Impact of primary  
713 formaldehyde on air pollution in the Mexico City Metropolitan Area, *Atmos. Chem. Phys.*, 9, 2607–2618,  
714 2009.

715 Liteplo, R.G., R. Beauchamp, M.E. Meek, and R. Chénier. Formaldehyde. Geneva: International  
716 Programme on Chemical Safety; 2002. [18 May 2010]. (Concise International Chemical Assessment  
717 Document 40) (<http://www.inchem.org/documents/cicads/cicads/cicad40.htm>).

718 Luecken, D.J., W.T. Hutzell, M.L. Strum, G.A. Pouliot, Regional sources of atmospheric formaldehyde and  
719 acetaldehyde, and implications for atmospheric modeling, *Atmospheric Environment* 47, 477-490,  
720 doi:10.1016/j.atmosenv.2011.10.005, 2012.

721 Meller, Richard, and Geert K Moortgat. Temperature dependence of the absorption cross sections of  
722 formaldehyde between 223 and 323 k in the wavelength range 225-375 nm. *Journal of Geophysical*  
723 *Research: Atmospheres* (19842012), 105(D6):70897101, 2000.

724

725 Park. Junsung, Hanlim Lee, Jhoon Kim, Jay Herman, Woogyung Kim, Hyunkee Hong, Wonei Choi,  
726 Jiwon Yang and Daewon Kim, HCHO column density retrieval using Pandora measurements in Seoul,  
727 Korea: Temporal characteristics and comparison with OMI measurement, *Remote Sens.*, 10, 173;  
728 doi:10.3390/rs10020173, 2018.

729

730 Platt, U., D. Perner, and H. W. Pätz, Simultaneous measurements of atmospheric CH<sub>2</sub>, O<sub>3</sub> and NO<sub>2</sub> by  
731 differential optical absorption, *J. Geophys. Res.* 84 (1979), 6329–6335, 1979.

732

733 Platt, U. Differential optical absorption spectroscopy (DOAS), *Air monitoring by Spectroscopic Techniques*  
734 (M. Sigrist, ed.), John Wiley & Sons, Inc., 1994, pp. 27–84. [6] U. Platt, D. Perner, and H. W. Pätz,  
735 Simultaneous measurements of atmospheric CH<sub>2</sub>, O<sub>3</sub> and NO<sub>2</sub> by differential optical absorption, *J.*  
736 *Geophys. Res.* 84 (1979), 6329–6335, 1994.

737

738 Richter D., P. Weibring, J. G. Walega, A. Fried, S. M. Spuler, M. S. Taubman: Compact highly sensitive  
739 multi-species airborne mid-IR spectrometer, *Appl. Phys. B*, doi: 10.1007/s00340-015-6038-8, 2015.

740 Russell, A. R., Perring, A. E., Valin, L. C., Bucsela, E. J., Browne, E. C., Wooldridge, P. J., and Cohen, R. C.: A  
741 high spatial resolution retrieval of NO<sub>2</sub> column densities from OMI: method and evaluation, *Atmos.*  
742 *Chem. Phys.*, 11, 8543-8554, 2011.

743 Segal-Rosenheimer, M., P. B. Russell, B. Schmid, J. Redemann, J. M. Livingston, C. J. Flynn, R. R. Johnson,  
744 S. E. Dunagan, Y. Shinozuka<sup>1</sup>, J. Herman, A. Cede, N. Abuhassan, J. M. Comstock, J. M. Hubbe, A.  
745 Zelenyuk<sup>3</sup>, and J. Wilson, (2014) Tracking elevated pollution layers with a newly developed

746 hyperspectral Sun/Sky spectrometer(4STAR): Results from the TCAP 2012 and 2013 campaigns, J.  
747 Geophys. Res. Atmos., 119, 2611–2628, doi:10.1002/2013JD020884, 2014.

748 Shinozuka, Y., et al. , Hyperspectral aerosol optical depths from TCAP flights, J. Geophys. Res. Atmos.,  
749 118, 12,180–12,194, doi:10.1002/2013JD020596, 2013.

750 Spinei, E., N. Abuhassan, A Cede, M. Tiefengraber, M. Mueller, J. Herman, N. Nowak, B. Poche, S. Choi,  
751 A. Whitehill, J. Szykman, V. Lukas, D. Williams, R. Long, Jin Liao, Jason St. Clair, Glenn Wolfe, Thomas  
752 Hanisco, Changmin Cho, Alan Fried, Petter Weibring, Dirk Richter, Robert Swap, James Walega, Pandora  
753 formaldehyde measurements during KORUS-AQ over Olympic Park and Taehwa (South Korea, April-June  
754 2016), (submitted to AMT), 2018.

755 Thuillier, G., L. Floyd, T.N. Woods, R. Cebula, E. Hilsenrath, M. Hersé, and D. Labs. Solar irradiance  
756 reference spectra for two solar active levels. *Advances in Space Research*, 34(2):256–261, 2004.

757 Vandaele, A.C., C. Hermans, P. C. Simon, M. Carleer, R. Colin, S. Fally, M. F. Mérienne, A. Jenouvrier, and  
758 B. Coquart. Measurements of the NO<sub>2</sub> absorption cross-section from 42,000 cm<sup>-1</sup> to 10,000 cm<sup>-1</sup> (238-  
759 1000 nm) at 220 K and 294 K. *Journal of Quantitative Spectroscopy and Radiative Transfer*, 59: 171–184,  
760 doi: 10.1016/S0022-4073(97)00168-4, 1998.

761 VanHoosier, Michael E. Solar ultraviolet spectral irradiance data with increased wavelength and  
762 irradiance accuracy. In SPIE's 1996 International Symposium on Optical Science, Engineering, and  
763 Instrumentation, pages 57–64. International Society for Optics and Photonics, 1996.

764 Walters, Wendell & Goodwin, Stanford & Michalski, Greg. (2015). The Nitrogen Stable Isotope  
765 Composition ( $\delta^{15}\text{N}$ ) of Vehicle Emitted NO<sub>x</sub>. *Environmental science & technology*. 49.  
766 10.1021/es505580v, 2015.

767 Zhang, Hongliang, Jingyi Li, Qi Ying, Birnur Buzcu Guven, and Eduardo P. Olaguer, Source apportionment  
768 of formaldehyde during TexAQs 2006 using a source-oriented chemical transport model, *J. Geophys.*  
769 *Res.*, 118, 1525–1535, doi:10.1002/jgrd.50197, 2013.

770 Zhu, Lei, Daniel J. Jacob, Frank N. Keutsch, Loretta J. Mickley, Richard Scheffe, Madeleine Strum, Gonzalo  
771 González Abad, Kelly Chance, Kai Yang, Bernhard Rappenglück, Dylan B. Millet, Munkhbayar Baasandorj,  
772 Lyatt Jaeglé, and Viral Shah, Formaldehyde (HCHO) As a Hazardous Air Pollutant: Mapping Surface Air  
773 Concentrations from Satellite and Inferring Cancer Risks in the United States, *Environmental Science &*  
774 *Technology* 51 (10), 5650-5657, DOI: 10.1021/acs.est.7b01356, 2017.

775

776

777

778

779 Acknowledgement

780 The author would like to thank the Pandora project for support in completing this study as well as  
781 financial support from the KORUS-AQ project NNH15ZDA001N-KORUS. Dr. Jae Kim and Dr. Jhoon  
782 Kim are supported by Korea Ministry of Environment as Public Technology Program based on  
783 Environmental Policy (2017000160001). All data is available from a NASA data repository:  
784 <https://avdc.gsfc.nasa.gov/pub/DSCOVER/Pandora/DATA/KORUS-AQ/>

785

786

787 **Tables**

Table 1 KORUS-AQ Locations (South to North)

Locations	Alt(m)	Latitude	Longitude
Gwangju	33	35.2260N	126.8430W
Busan	228	35.2353N	129.0825W
Anmyeondo	41	36.5380N	126.3300W
Taehwa Mtn	160	37.3123N	127.3106W
Yeosu-1 & 2	90	37.3385N	127.4895W
Songchon	49	37.4100N	127.5600W
Olympic Park	26	37.5232N	127.1260W
Seoul	181	37.5644N	126.9340W

788

789

Table 2 Taehwa Mtn DC8 compared to PSI measurements in Fig. 18

Date	LT	DC8 HCHO DU	PSI HCHO	Percent
11 May	08:25:19	0.4	0.6	67
18 May	08:34:26	0.4	0.5	80
30 May	12:05:00	0.5	0.9	56
10 Jun	08:22:45	1	1.16	86
10 Jun	12:22:53	1	1.5	67
10 Jun	15:46:03	1	1.3	77

790

791



792 **Figure Captions**

793 **Fig. 1** KORUS-AQ sites for 9 Pandora instruments at 8 sites.

794 **Fig. 2a** C(NO<sub>2</sub>) amounts from Pandora 27 and 35 in Yeosu, Korea during 3 June 2016 and their difference  
795 |Pan35 – Pan27| < 0.05 DU.

796 **Fig. 2b** Pandora 35 estimate of cloud or aerosol reduced measured counts/second at approximately 500  
797 nm.

798 Fig. 3. Frequency distributions of C(NO<sub>2</sub>) across the KORUS-AQ PSI network: April 20 to Jun 6 2016,  
799 except as labelled. The axes vary for different sites.

800 Fig. 4 NO<sub>2</sub> time series vs day of the year (DOY) and diurnal variability (daily vertical extent) at 9 Pandora  
801 sites. Notice the very high NO<sub>2</sub> amounts in Seoul and nearby Olympic Park. The black curves are  
802 approximately weekly least squares running averages. Note: the vertical scales are different for each site  
803 to show the daily variability relative to the running average.

804 Fig. 5 NO<sub>2</sub> amounts vs Day of the Year (DOY) and Local Time for six sites as labeled in each panel. Day  
805 120=April 29, Day 130=May 9, Day 140=May 19, Day 150=May 29, Day 160=June 8, Day 170 =June18.

Fig. 6 Approximately 1 year of daily column C(NO<sub>2</sub>) amount data (Panels A and D) and the monthly  
running average amount (dark plot in Panels A and D). The data are from GIST at Gwangju and  
Amnyeondo. Panels A and D are the original time series with one data point every 80 seconds, panels B  
and E are the deseasonalized time series. Panels C and F are an expanded scale of the monthly running  
averages  $M(t)$  of C(NO<sub>2</sub>) that are identical to the solid lines in panels A and D. The vertical extent (panels  
A, B, D, and E) on a given day is the range of diurnal variation from early morning to late afternoon.

806 Fig. 7 (A) NO<sub>2</sub> time series at Yonsei University in Seoul NO<sub>2</sub>(grey) and (B) deseasonalized time series.  
807 Combined slope =  $-0.05 \pm 0.001$  DU/Year and Mean =  $1.2 \pm 0.8$  DU or the decrease is  $-4 \pm 0.08$  % / Year.  
808 Seoul has no clear seasonal cycle.

809 Fig. 8 (A) Pusan University in Busan NO<sub>2</sub> daily time series (grey) and (B) deseasonalized time series with  
810 linear trends.

811 Fig. 9a Comparisons between the daily values of C(NO<sub>2</sub>) for OMI (black) and PSI (red) at Seoul and Busan  
812 for a 5-year period. Solid lines show the average seasonal variation (Lowess(0.1)), see also Fig. 9b. Linear  
813 interpolation is used where there are missing data points.

814 Fig. 9b Comparisons between the seasonal averages for C(NO<sub>2</sub>) from OMI (black) and PSI (red) at Seoul  
815 and Busan for a 5-year period. The lower panels show the seasonal difference between the PSI and  
816 OMI. The individual data points are shown derived from a Lowess(0.1) smoothing, approximately a 3-  
817 month running averages of the daily data. Interpolation has been used where there are missing data  
818 points.

819 Fig. 10 C(NO<sub>2</sub>) time series from Pandora (red) and OMI (black) for GIST University in Gwangju Korea and  
820 their differences. The comparison is formed from time coincidences between Pandora and OMI.

821 Fig. 11 A correlation plot of C(NO<sub>2</sub>) from 4STAR onboard the DC-8 compared to the C(NO<sub>2</sub>) amount  
822 measured by the PSI at Olympic Park on nine different days. The solid black line is the 1:1 line drawn for  
823 reference. The dashed line represents the data linear fit, with a slope of 1.05, and a correlation  
824 coefficient  $r^2 = 0.7$ , as shown on the plot.

825 Fig. 12 C(HCHO) from PSI at Olympic Park for 6 days in June 2016. C(HCHO) on 2 June 2016 has a peak  
826 value of 2.3 DU at 14:30 hours.

827 Fig. 13 Pandora measured formaldehyde amounts vs day of the year and local time for 29 April 2016 to  
828 11 June 2016 in Olympic Park.

829 Fig. 14 HCHO altitude profile measured onboard the DC8 on 4 May at 07:54 (A) and 11:54 (B) local time  
830 over Olympic Park, Korea. Panel C: PSI measurements of total column HCHO. Vertical bars mark the DC8  
831 flight duration for the profiles yielding altitude integrated column amounts of 0.38 and 0.26 DU.

832 Fig. 15 DC-8 HCHO measurements over Olympic Park on June 4. The continuous blue profiles  
833 show the 1-second HCHO data while the black points with error bars show the 10-second  
834 average and standard deviation of this data at points of closest approach above the Olympic  
835 Park site.

836 Fig. 16 HCHO altitude profile measured onboard the DC8 on 5 June at 8:30 (A) and 15:21 (B) local time  
837 over Olympic Park, Korea. Panel C: PSI measurements of total column HCHO. Vertical bars mark the DC8  
838 flight duration for the profiles yielding column amounts of 0.60 and 0.82 DU.

839 Fig. 17 Total column HCHO from Pandora Yonsei University, Seoul for 6 days in June 2016. HCHO on 2  
840 June 2016 has a peak value of 1.2 DU at 13:30 hours.

841 Fig. 18 Total column HCHO from Pandora Taehwa Mountain for 6 days in June 2016. HCHO on 2 June  
842 2016 has a peak value of 1.2 DU at 12:45.  $\Delta$  are DC8 measurements on 10 June.

843 Fig. 19a Summary of total column HCHO for the stated dates during the KORUS-AQ campaign. The solid  
844 line is a Lowess(0.1) fit to the data. The sharp cutoffs in panel A, B, and C were caused obstructions of  
845 the direct sun from the PSI FOV in the afternoon.

846 Fig. 19b Summary of total column HCHO for the stated dates during the KORUS-AQ campaign. Panels A  
847 and B represent the daily variation at a given local time. The solid line is a Lowess(0.1) fit to the data.  
848 Panels C and D show the frequency of occurrence (%) for different amounts of HCHO.

849 Fig. 20 The springtime change in C(HCHO) over about a 40 day period depending on the site.  
850 The “vertical bars” are the diurnal variation within each day of data. The thicker red curve is a  
851 Lowess(0.3) fit to the data, while the thin red line is a linear least squares fit. The Lowess(0.3) fit  
852 is approximately a 10-day local least-squares average.

853 Fig. 21 Compare PSI • and OMI o retrievals of C(HCHO) at  $13.5 \pm 0.5$  hours. OMI overpass data, V03, are  
854 from <https://avdc.gsfc.nasa.gov/index.php?site=1113974256&id=81>

855 Fig. A1 An illustration of the deseasonalization (right panel) of the monthly running average of NO<sub>2</sub> for  
856 the Gwangju site (left panel) shown in Fig. 6. The insets are magnifications of the main plots.

857

858

859 Figures

860

861

862

863

864

865

866

867

868

869

870

871



872

**Fig. 1** KORUS-AQ sites for 9 Pandora instruments at 8 sites.

873

874

875

876 **F01**

877

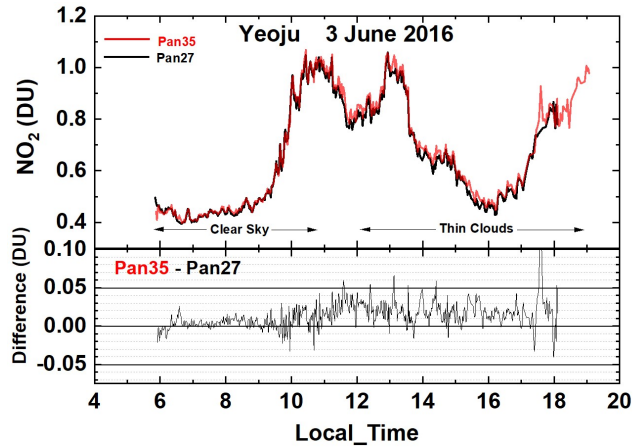


**Fig. 2a**  $C(\text{NO}_2)$  amounts from Pandora 27 and 35 in Yeosu, Korea during 3 June 2016 and their difference  $|\text{Pan35} - \text{Pan27}| < 0.05$  DU.

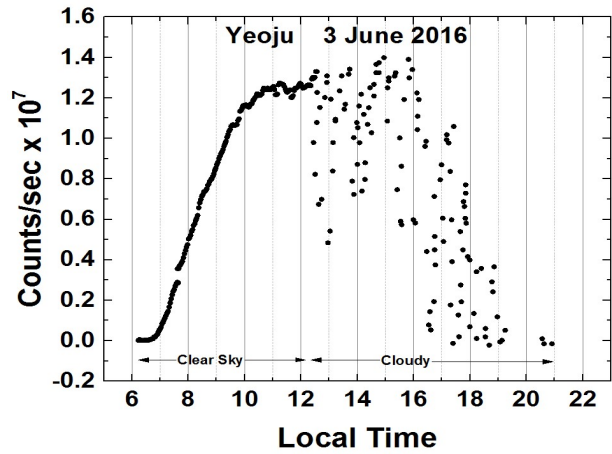


**Fig. 2b** Pandora 35 estimate of cloud or aerosol reduced measured counts/second at approximately 500 nm.

878

879 **F02**

880

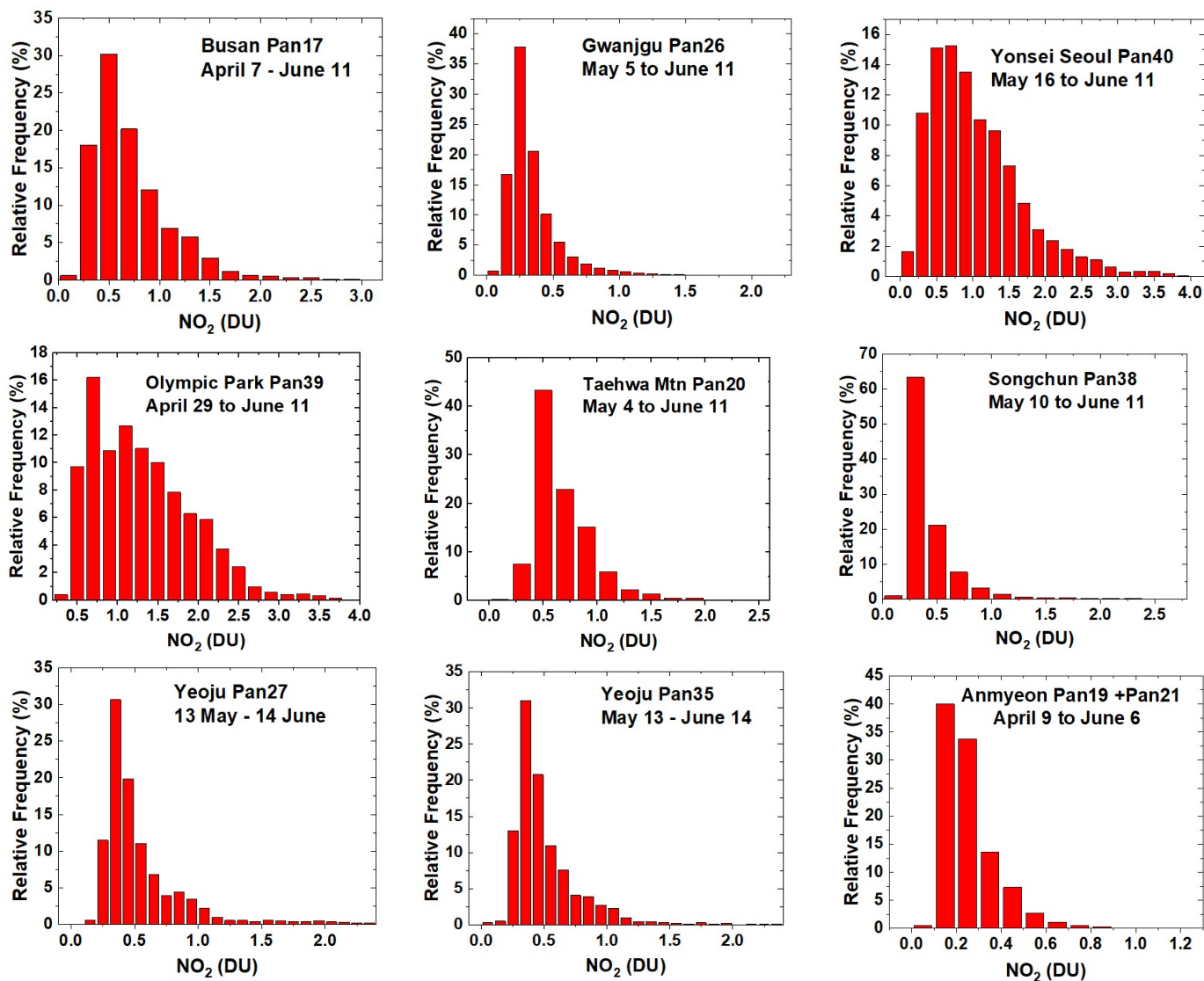


Fig. 3. Frequency distributions of  $C(\text{NO}_2)$  across the KORUS-AQ PSI network: April 20 to Jun 6 2016, except as labelled. The axes vary for different sites.

881

882 **F03**

883

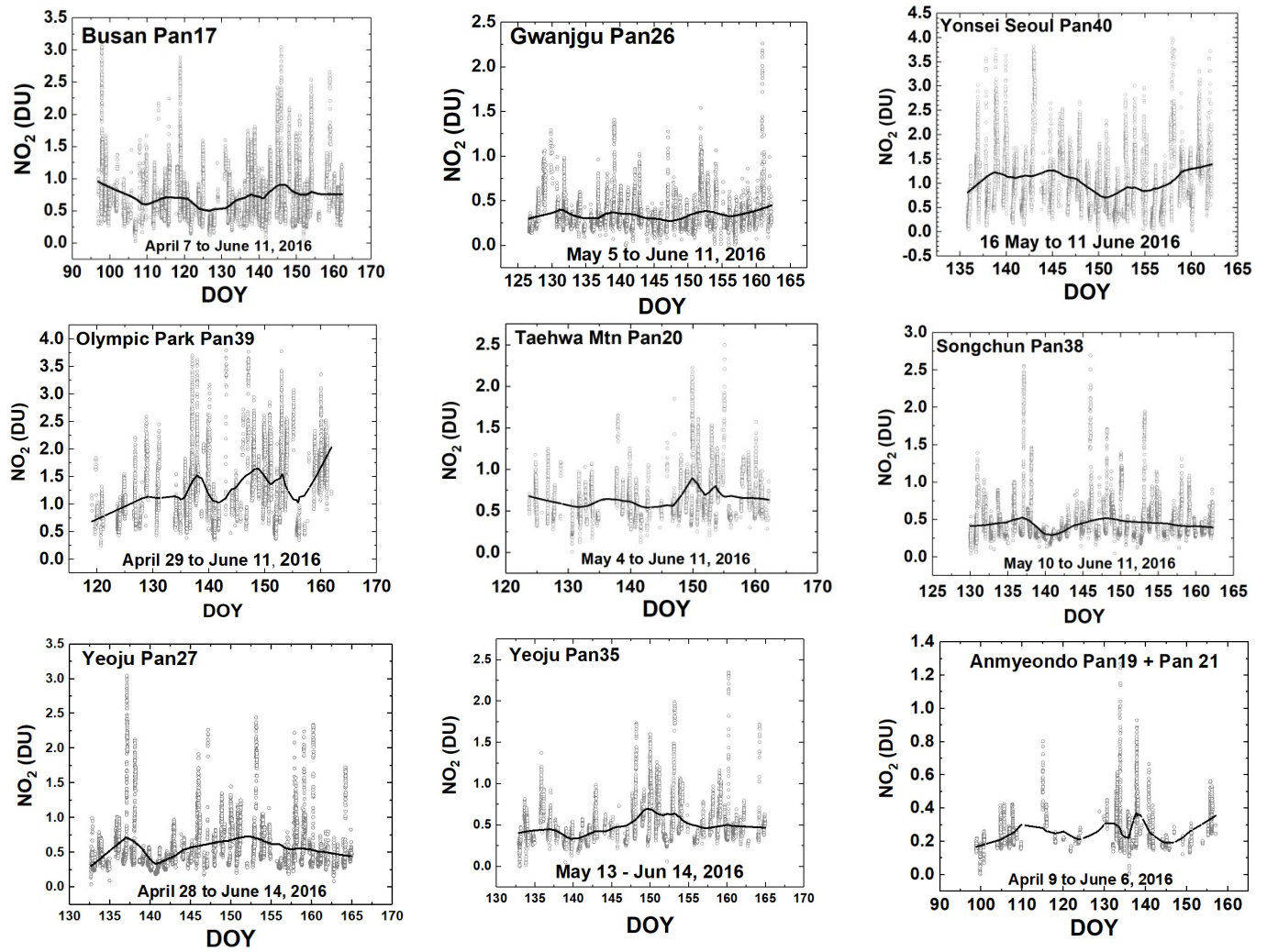


Fig. 4 NO<sub>2</sub> time series vs day of the year (DOY) and diurnal variability (daily vertical extent) at 9 Pandora sites. Notice the very high NO<sub>2</sub> amounts in Seoul and nearby Olympic Park. The black curves are approximately weekly least squares running averages. The daily vertical extent corresponds to diurnal variation (Fig. 2). Note: the vertical scales are different for each site to show the daily variability relative to the running average.

884

885 **F04**

886

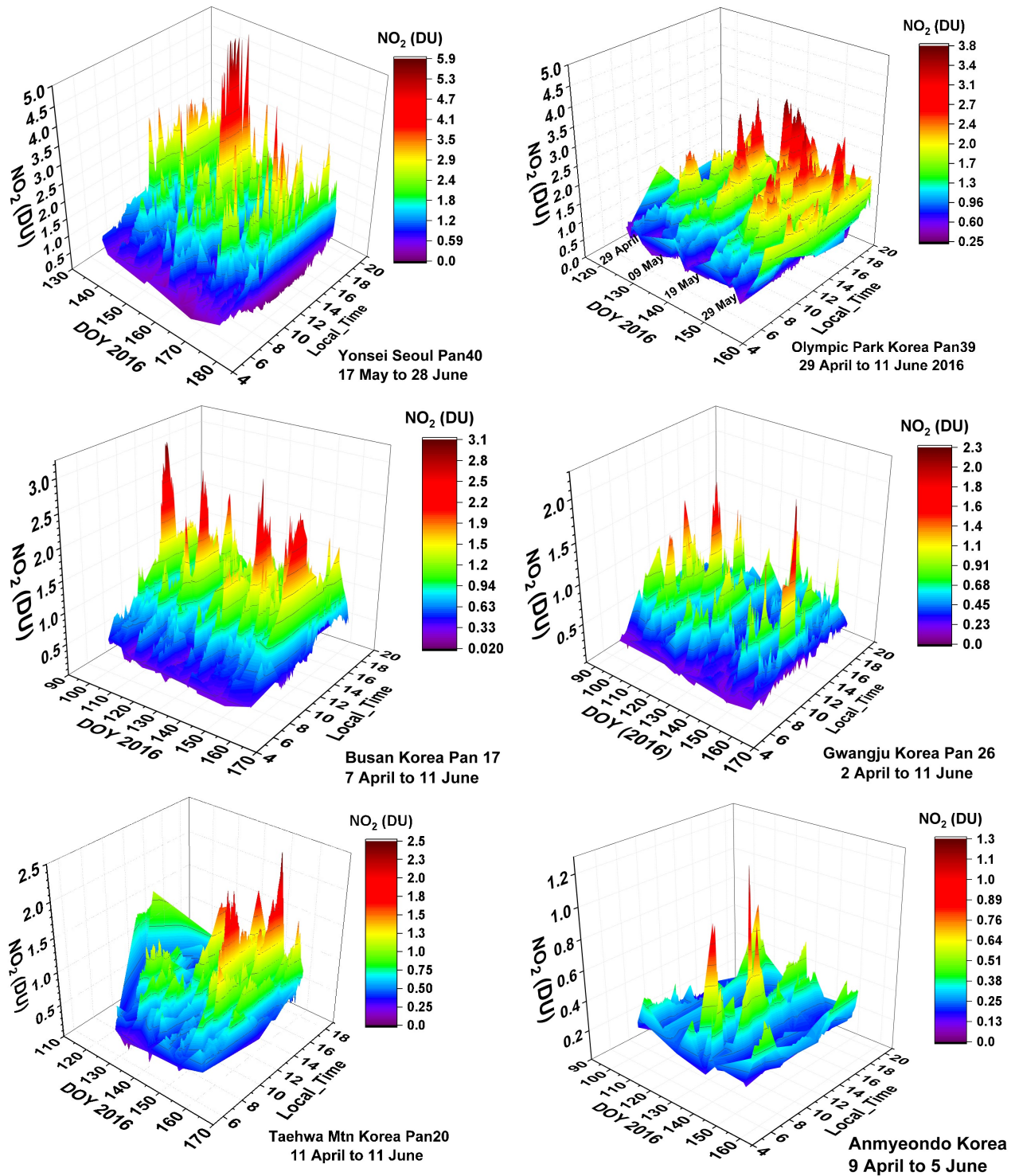


Fig. 5 NO<sub>2</sub> amounts vs Day of the Year (DOY) and Local Time for six sites as labeled in each panel. Day 120=April 29, Day 130=May 9, Day 140=May 19, Day 150=May 29, Day 160=June 8, Day 170 =June18.

887

888 **F05**



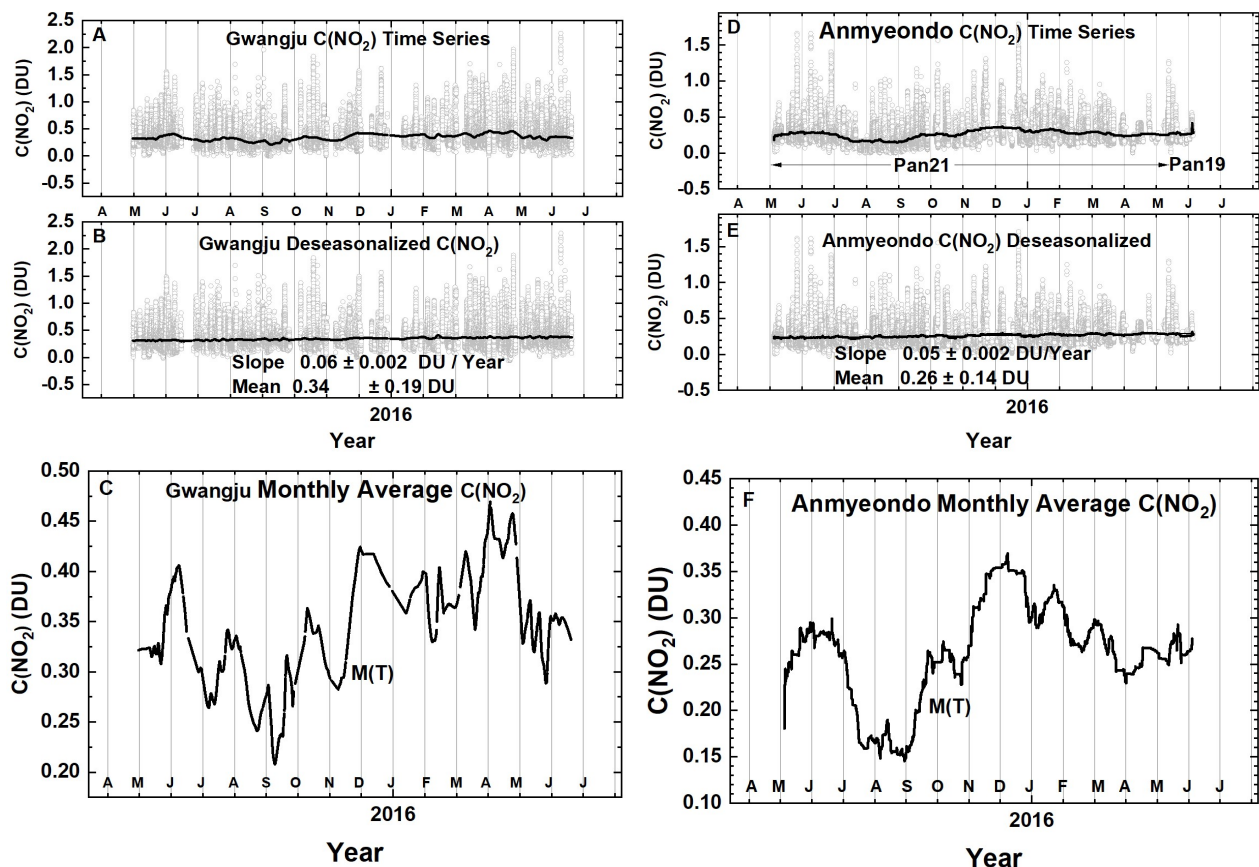


Fig. 6 Approximately 1 year of daily column  $C(\text{NO}_2)$  amount data (Panels A and D) and the monthly running average amount (dark plot in Panels A and D). The data are from GIST at Gwangju and Anmyeondo. Panels A and D are the original time series with one data point every 80 seconds, panels B and E are the deseasonalized time series. Panels C and F are an expanded scale of the monthly running averages  $M(t)$  of  $C(\text{NO}_2)$  that are identical to the solid lines in panels A and D. The vertical extent (panels A, B, D, and E) on a given day is the range of diurnal variation from early morning to late afternoon.

889

890

891 **F06**

892

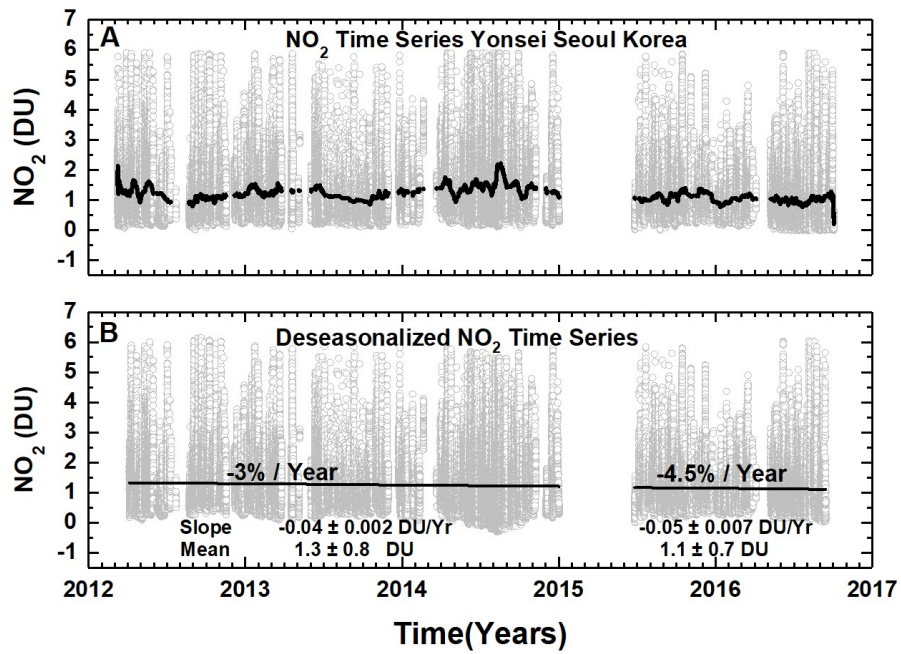


Fig. 7 (A) NO<sub>2</sub> time series at Yonsei University in Seoul NO<sub>2</sub>(grey) and (B) deseasonalized time series. Combined slope =  $-0.05 \pm 0.001$  DU/Year and Mean =  $1.2 \pm 0.8$  DU or the decrease is  $-4 \pm 0.08$  % / Year. Seoul has no clear seasonal cycle.

893

894 **F07**

895

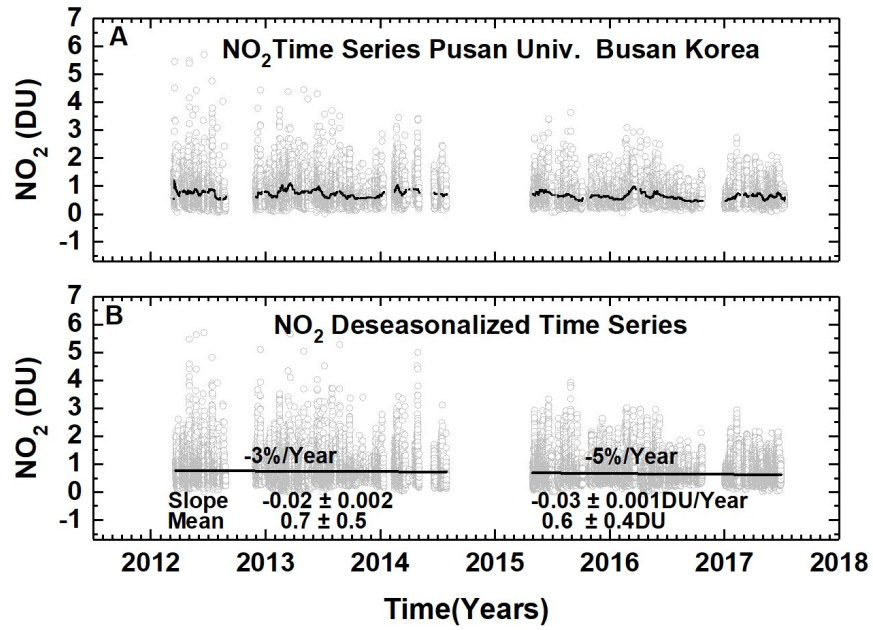


Fig. 8 (A) Pusan University in Busan NO<sub>2</sub> daily time series (grey) and (B) deseasonalized time series with linear trends.

896

897 **F08**

898

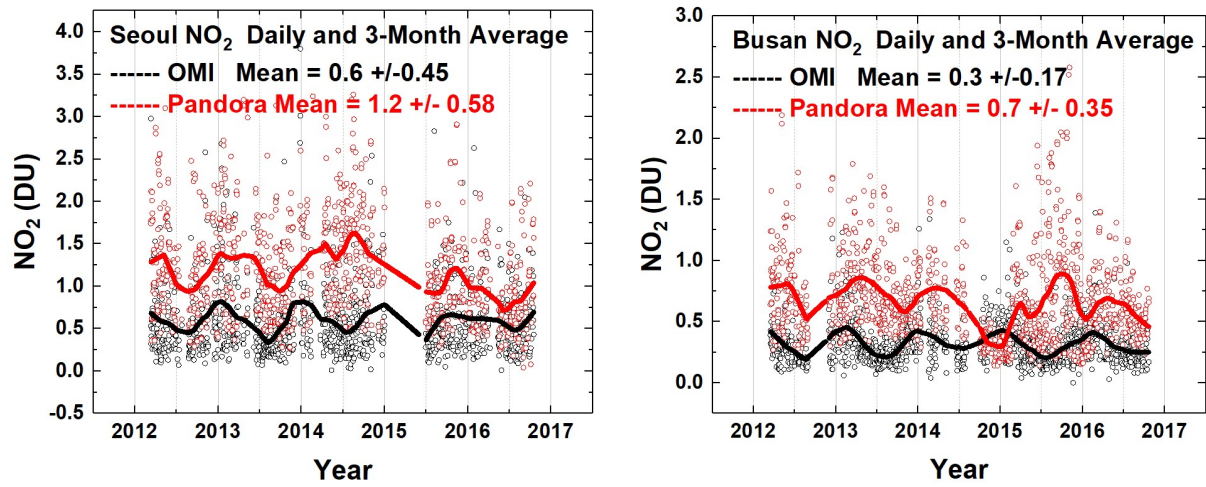


Fig. 9a Comparisons between the daily values of C(NO<sub>2</sub>) for OMI (black) and PSI (red) at Seoul and Busan for a 5-year period. Solid lines show the average seasonal variation (Lowess(0.1)), see also Fig. 9b. Linear interpolation is used where there are missing data points.

899

900 **F09a**

901

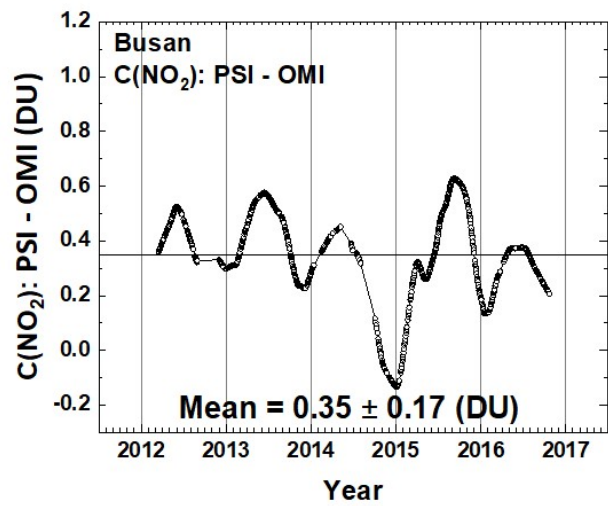
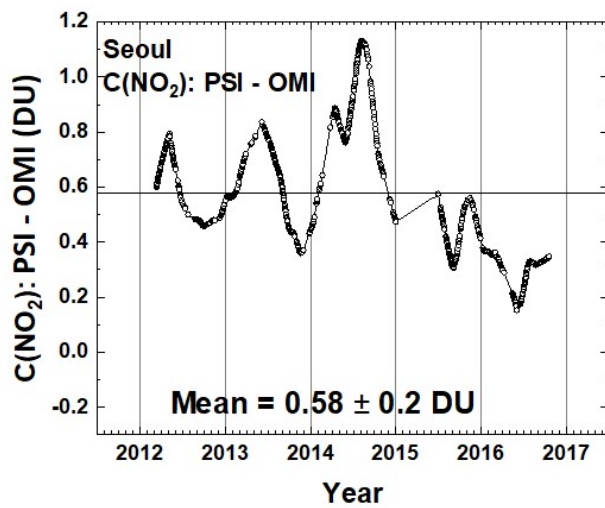
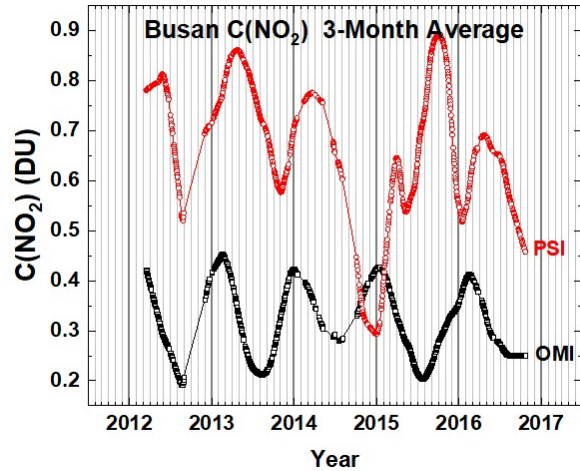
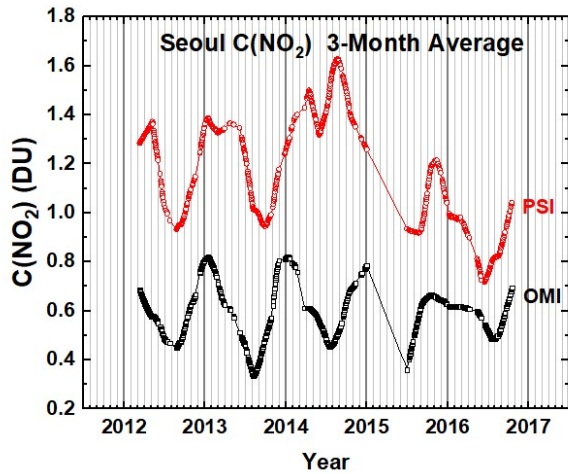


Fig. 9b Comparisons between the seasonal averages for  $C(\text{NO}_2)$  from OMI (black) and PSI (red) at Seoul and Busan for a 5-year period. The lower panels show the seasonal difference between the PSI and OMI. The individual data points are shown derived from a Lowess(0.1) smoothing, approximately a 3-month running averages of the daily data. Interpolation has been used where there are missing data points.

902

903 **F09b**

904

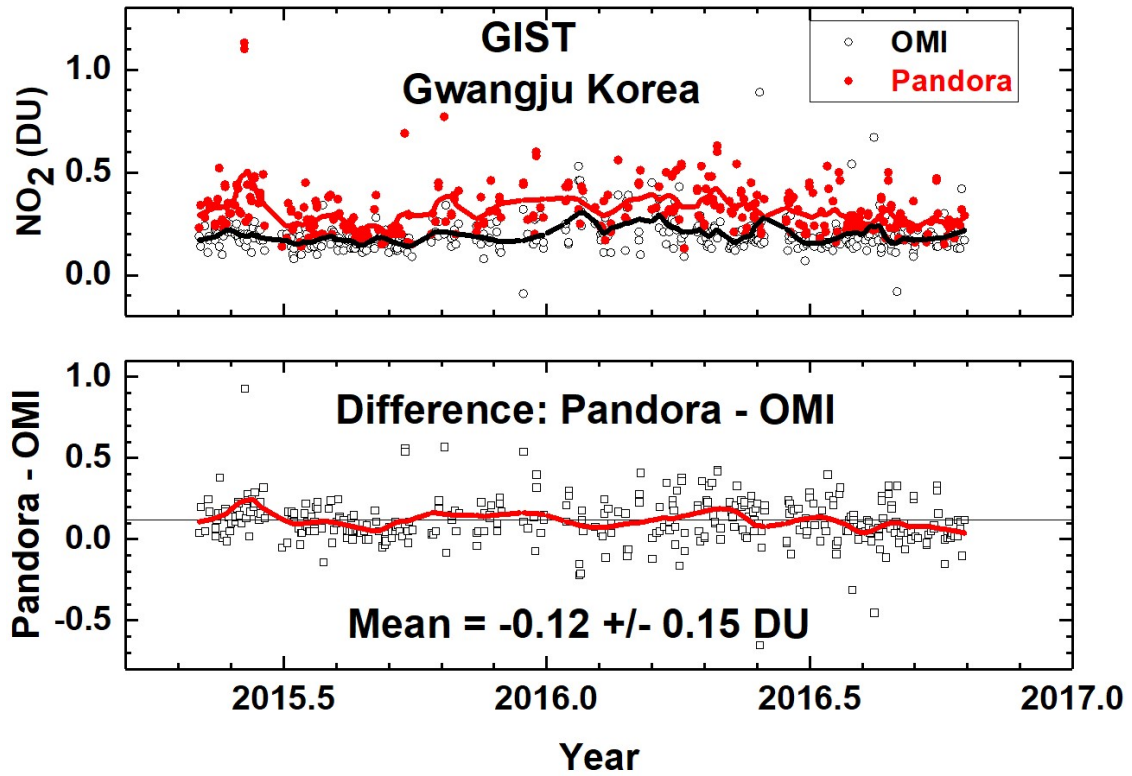


Fig. 10 C(NO<sub>2</sub>) time series from Pandora (red) and OMI (black) for GIST University in Gwangju Korea and their differences. The comparison is formed from time coincidences between Pandora and OMI.

905

906 **F10**

907

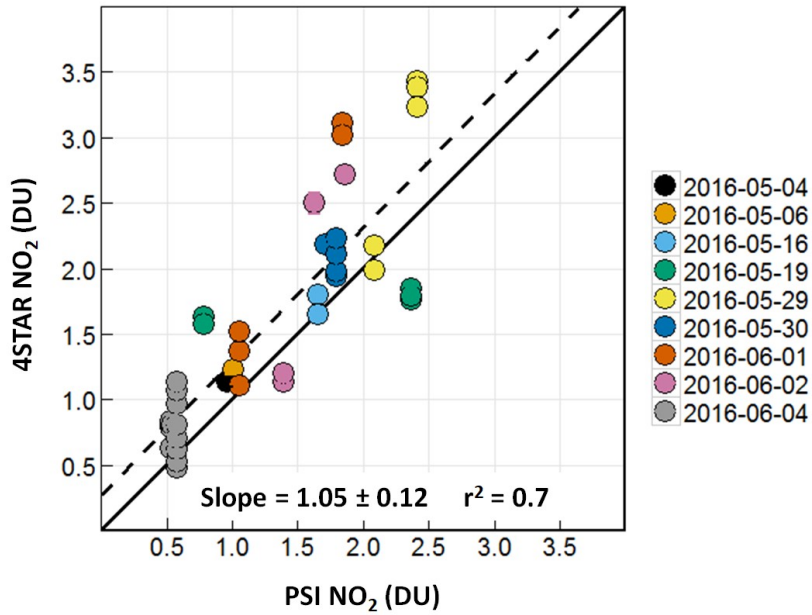


Fig. 11 A correlation plot of C(NO<sub>2</sub>) from 4STAR onboard the DC-8 compared to the C(NO<sub>2</sub>) amount measured by the PSI at Olympic Park on nine different days. The solid black line is the 1:1 line drawn for reference. The dashed line represents the data linear fit, with a slope of 1.05, and a correlation coefficient  $r^2 = 0.7$ , as shown on the plot.

908

909 **F11**

910

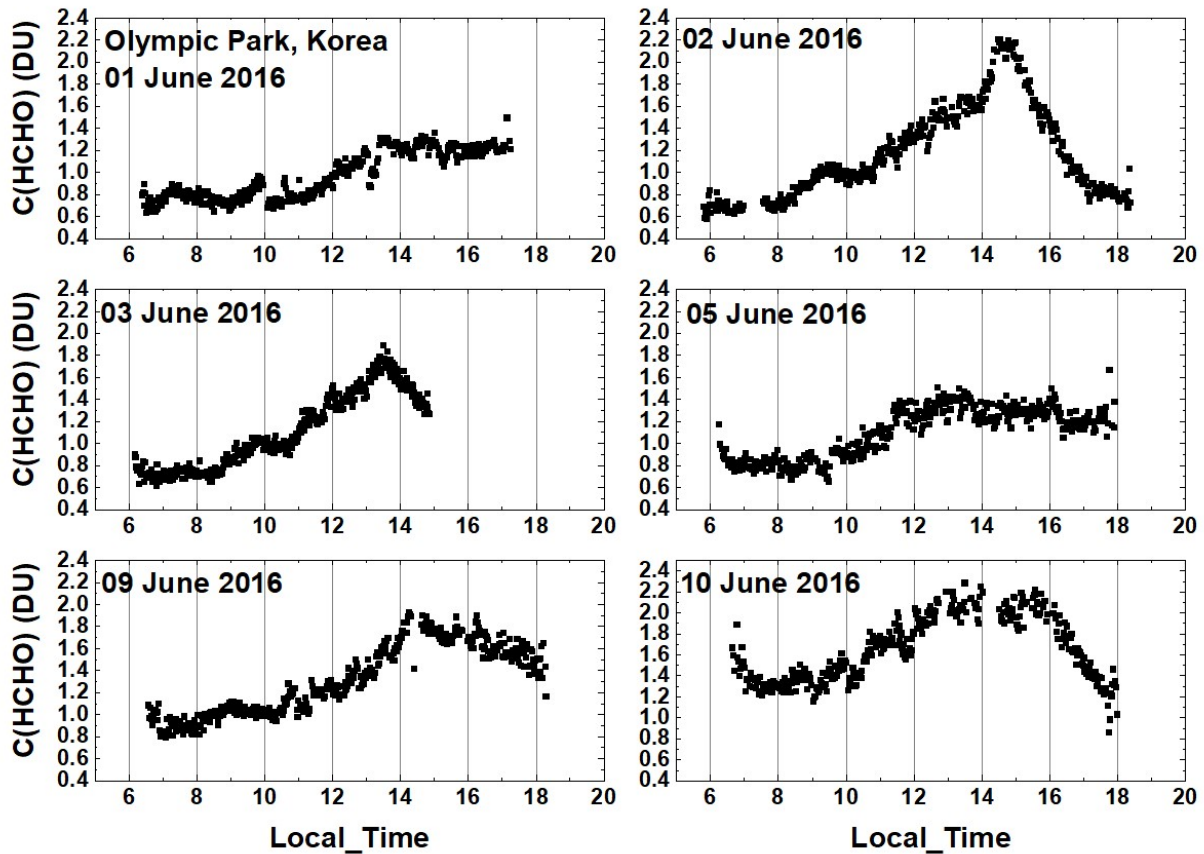


Fig. 12 C(HCHO) from PSI at Olympic Park for 6 days in June 2016. C(HCHO) on 2 June 2016 has a peak value of 2.3 DU at 14:30 hours.

911

912 **F12**

913

914



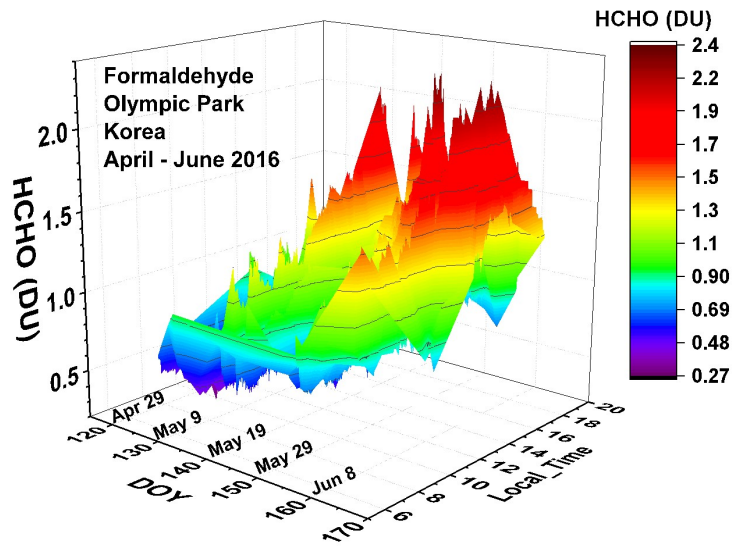


Fig. 13 Pandora measured formaldehyde amounts vs day of the year and local time for 29 April 2016 to 11 June 2016 in Olympic Park.

915

916 **F13**

917

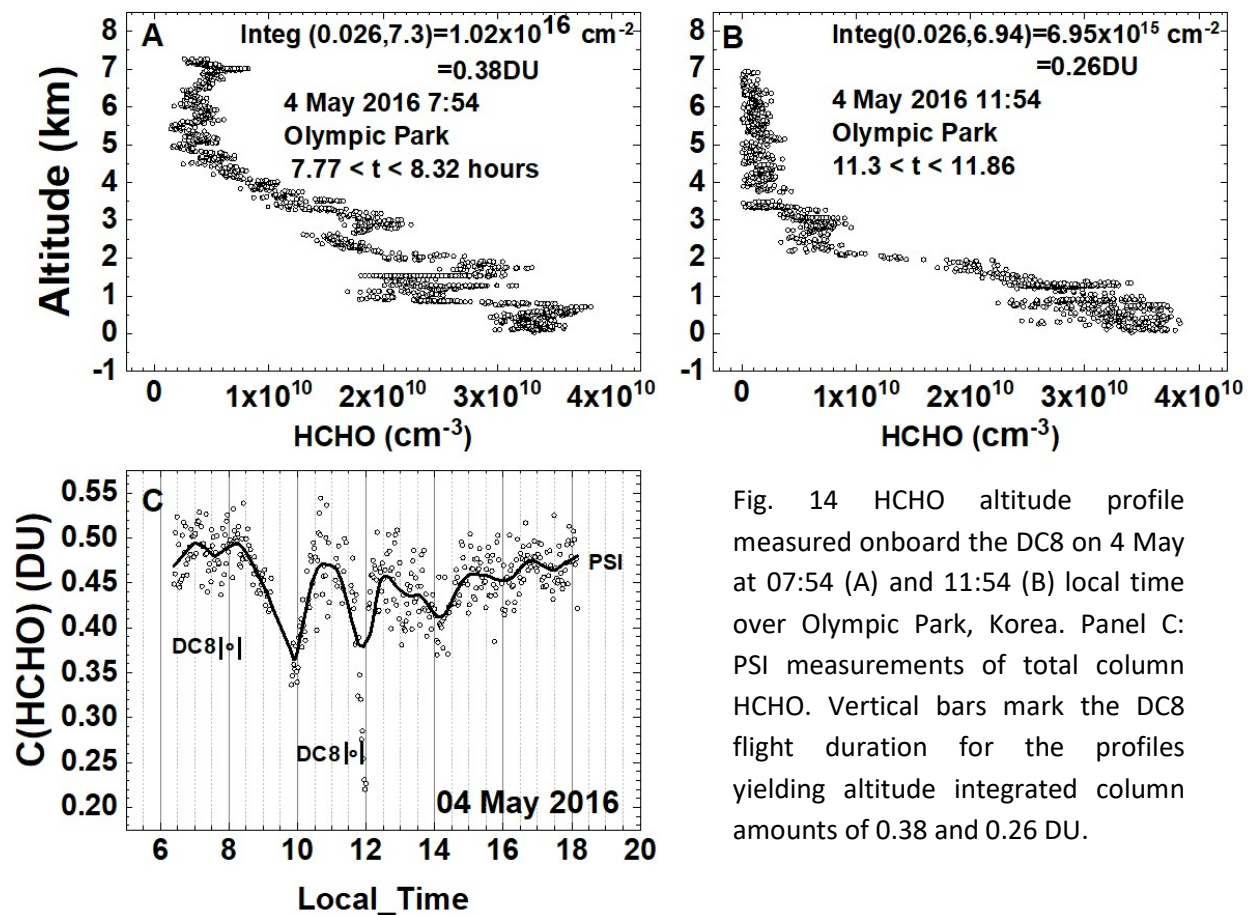


Fig. 14 HCHO altitude profile measured onboard the DC8 on 4 May at 07:54 (A) and 11:54 (B) local time over Olympic Park, Korea. Panel C: PSI measurements of total column HCHO. Vertical bars mark the DC8 flight duration for the profiles yielding altitude integrated column amounts of 0.38 and 0.26 DU.

918

919 **F14**

920

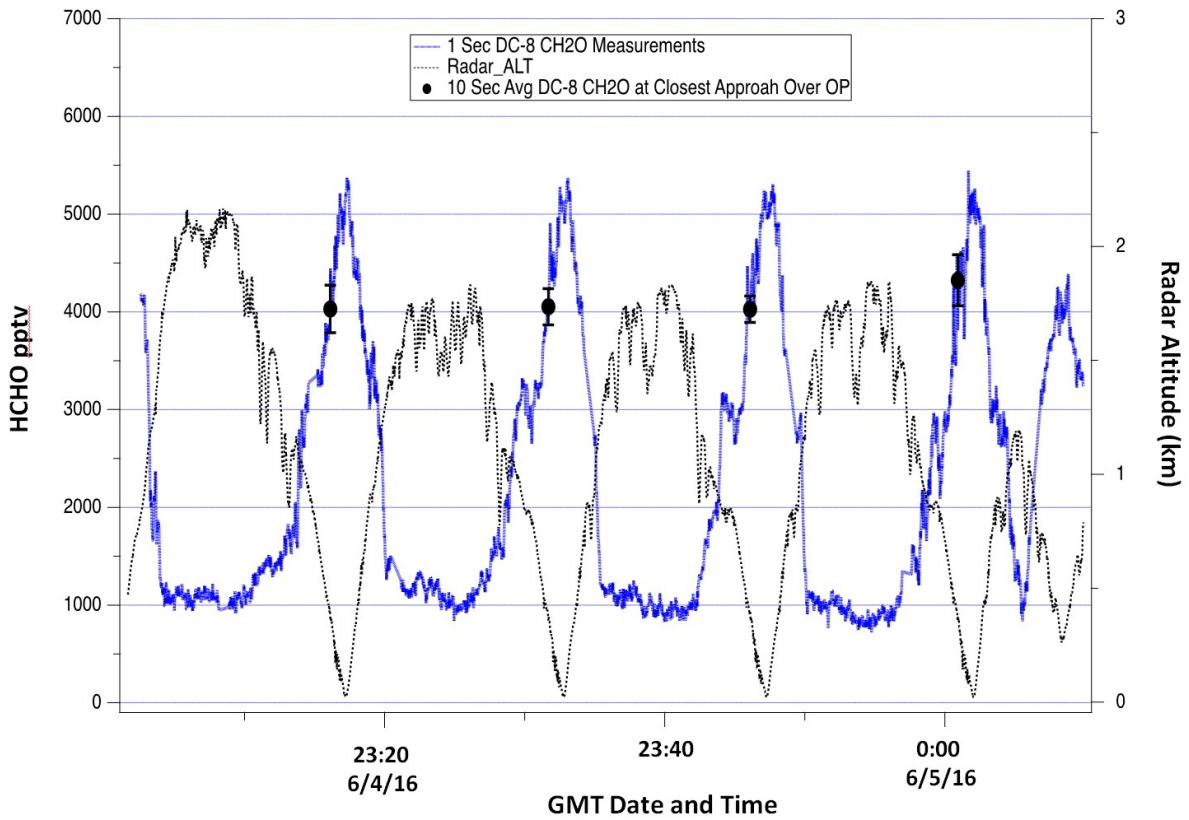


Fig. 15 DC-8 HCHO measurements over Olympic Park on June 4. The continuous blue profiles show the 1-second HCHO data while the black points with error bars show the 10-second average and standard deviation of this data at points of closest approach above the Olympic Park site.

921

922 **F15**

923

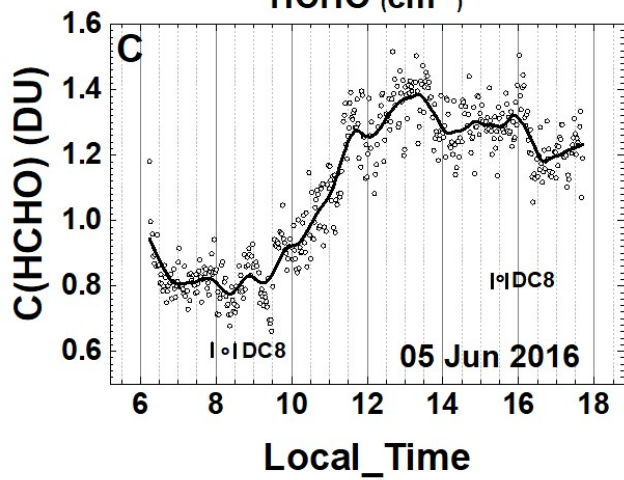
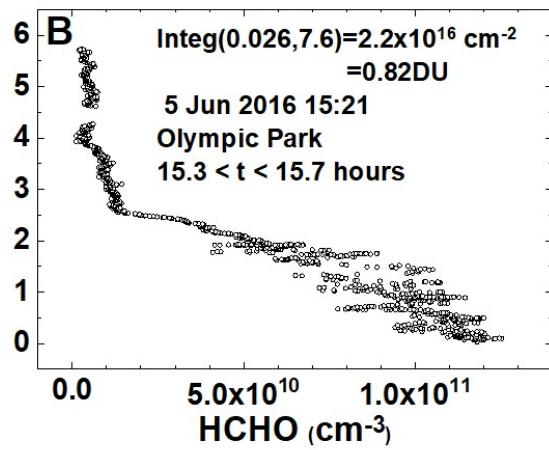
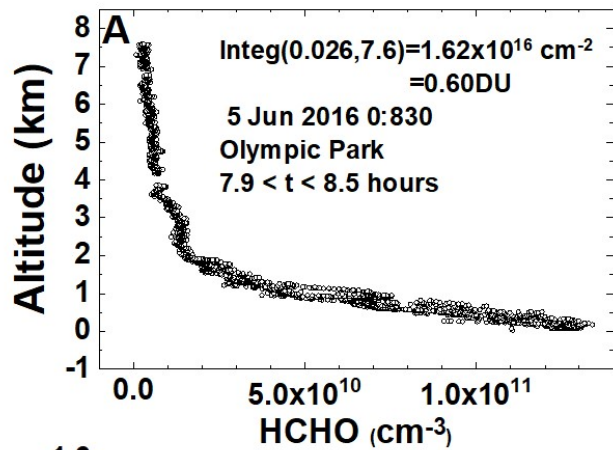


Fig. 16 HCHO altitude profile measured onboard the DC8 on 5 June at 8:30 (A) and 15:21 (B) local time over Olympic Park, Korea. Panel C: PSI measurements of total column HCHO. Vertical bars mark the DC8 flight duration for the profiles yielding column amounts of 0.60 and 0.82 DU.

924

925 **F16**

926

927

928

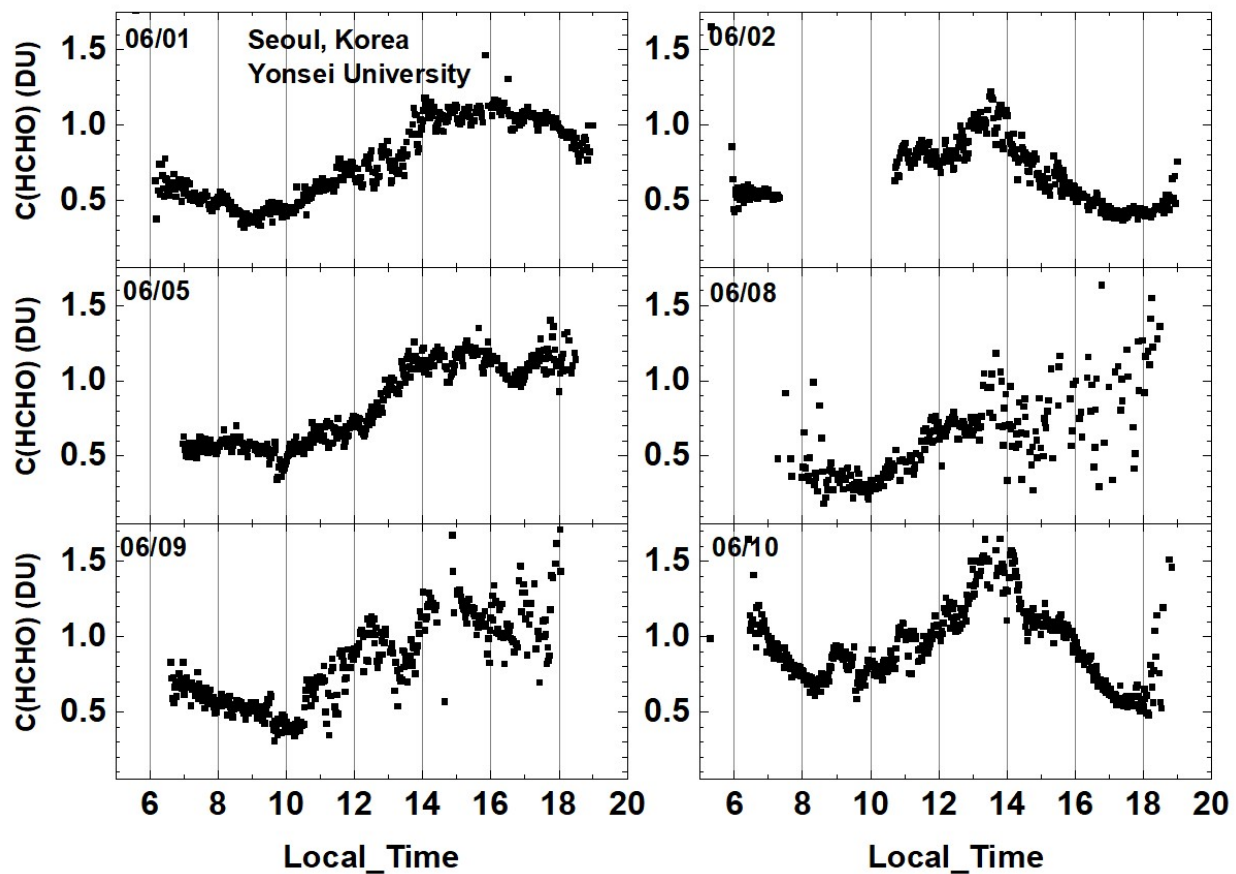


Fig. 17 Total column HCHO from Pandora Yonsei University, Seoul for 6 days in June 2016. C(HCHO) on 2 June 2016 has a peak value of 1.2 DU at 13:30 hours.

929

930 **F17**

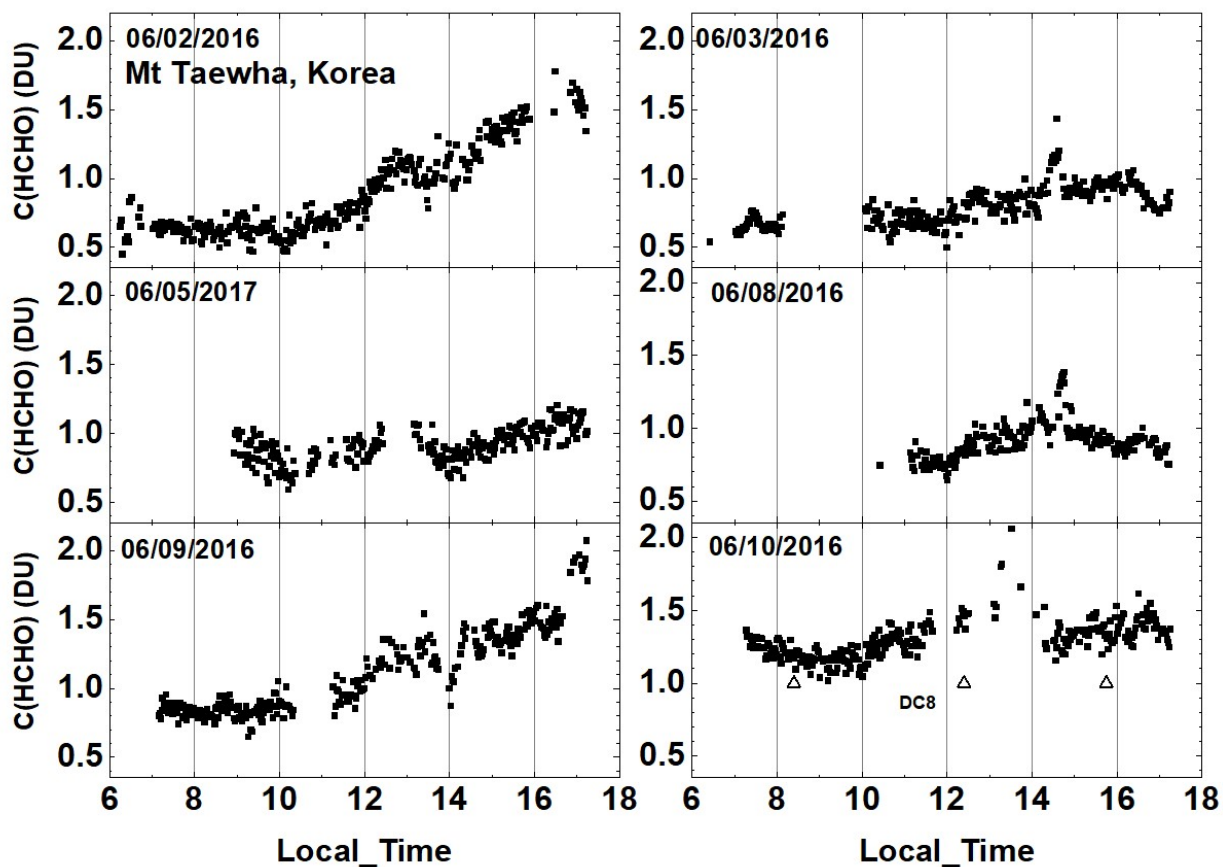


Fig. 18 Total column HCHO from Pandora at Taehwa Mountain for 6 days in June 2016. C(HCHO) on 2 June 2016 has a peak value of 1.7 DU at 16:20.  $\Delta$  are DC8 measurements on 10 June

931

932 **F18**

933

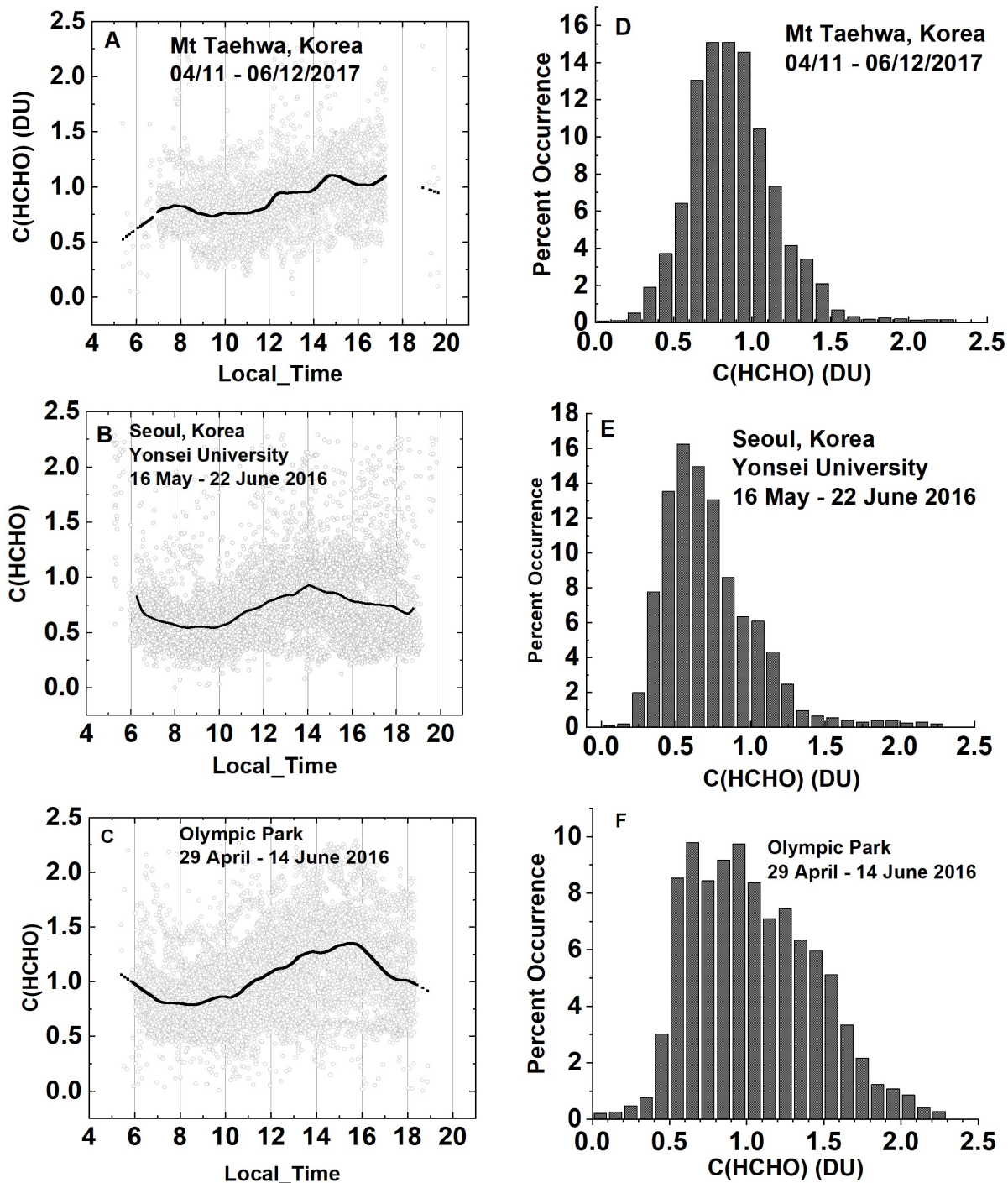


Fig. 19a Summary of total column HCHO for the stated dates during the KORUS-AQ campaign. The solid line is a Lowess(0.1) fit to the data. The sharp cutoffs in panel A, B, and C were caused by obstructions of the direct sun from the PSI FOV in the afternoon.

934

935 **F19a**

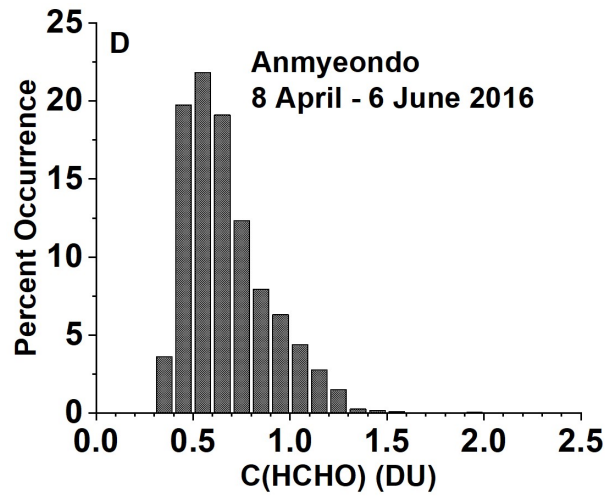
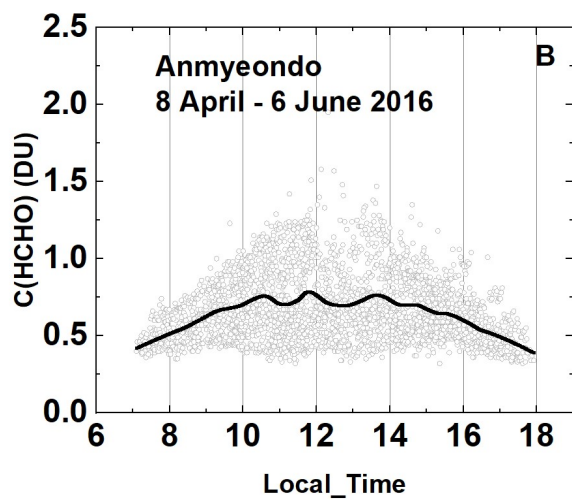
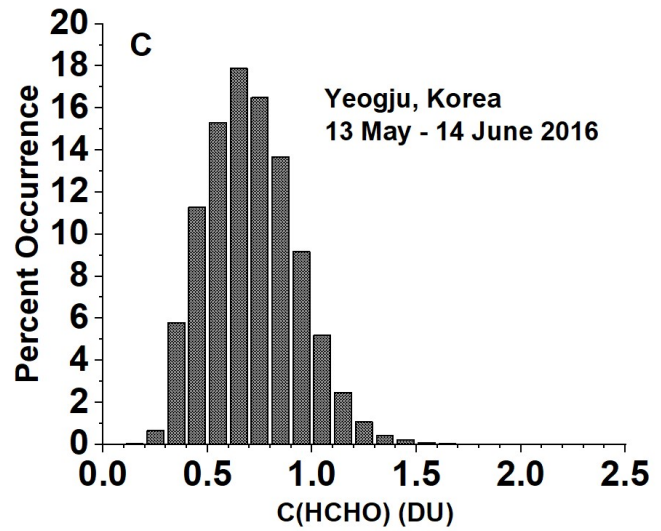
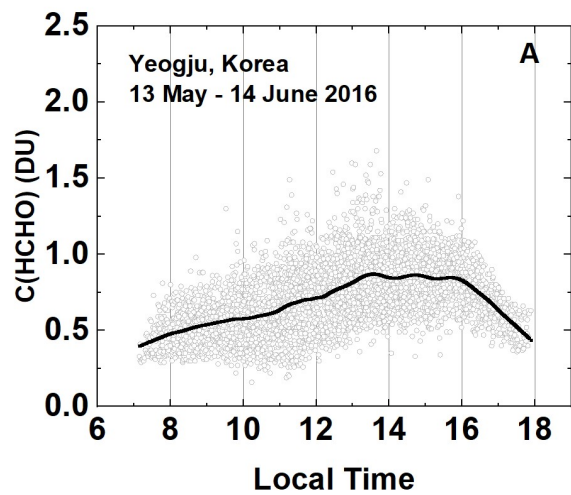


Fig. 19b Summary of total column HCHO for the stated dates during the KORUS-AQ campaign. Panels A and B represent the daily variation at a given local time. The solid line is a Lowess(0.1) fit to the data. Panels C and D show the frequency of occurrence (%) for different amounts of HCHO.

936

937

938 **F19b**

939



940

941

942

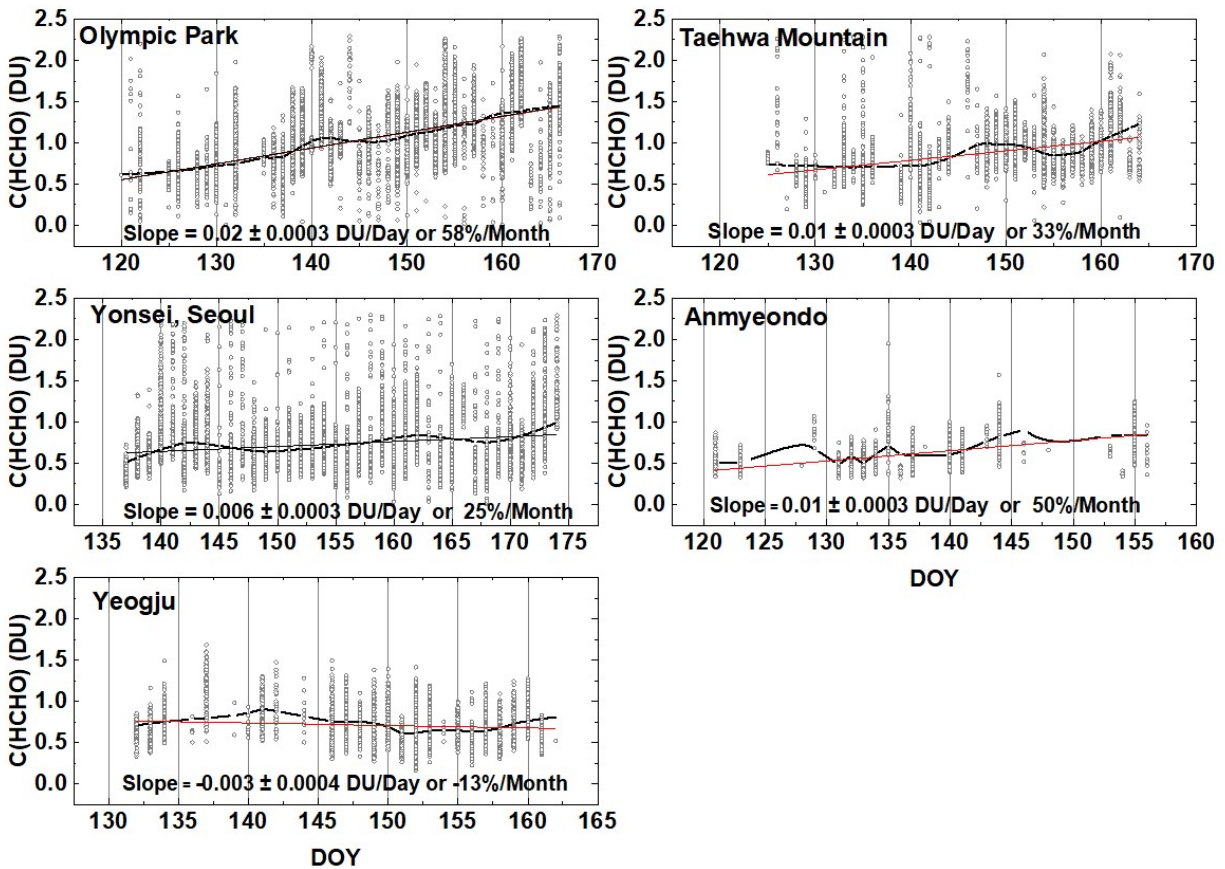


Fig. 20 The springtime change in C(HCHO) over about a 40 day period depending on the site. The “vertical bars” are the diurnal variation within each day of data. The thicker red curve is a Lowess(0.3) fit to the data, while the thin red line is a linear least squares fit. The Lowess(0.3) fit is approximately a 10-day local least-squares average.

943

944 **F20**

945

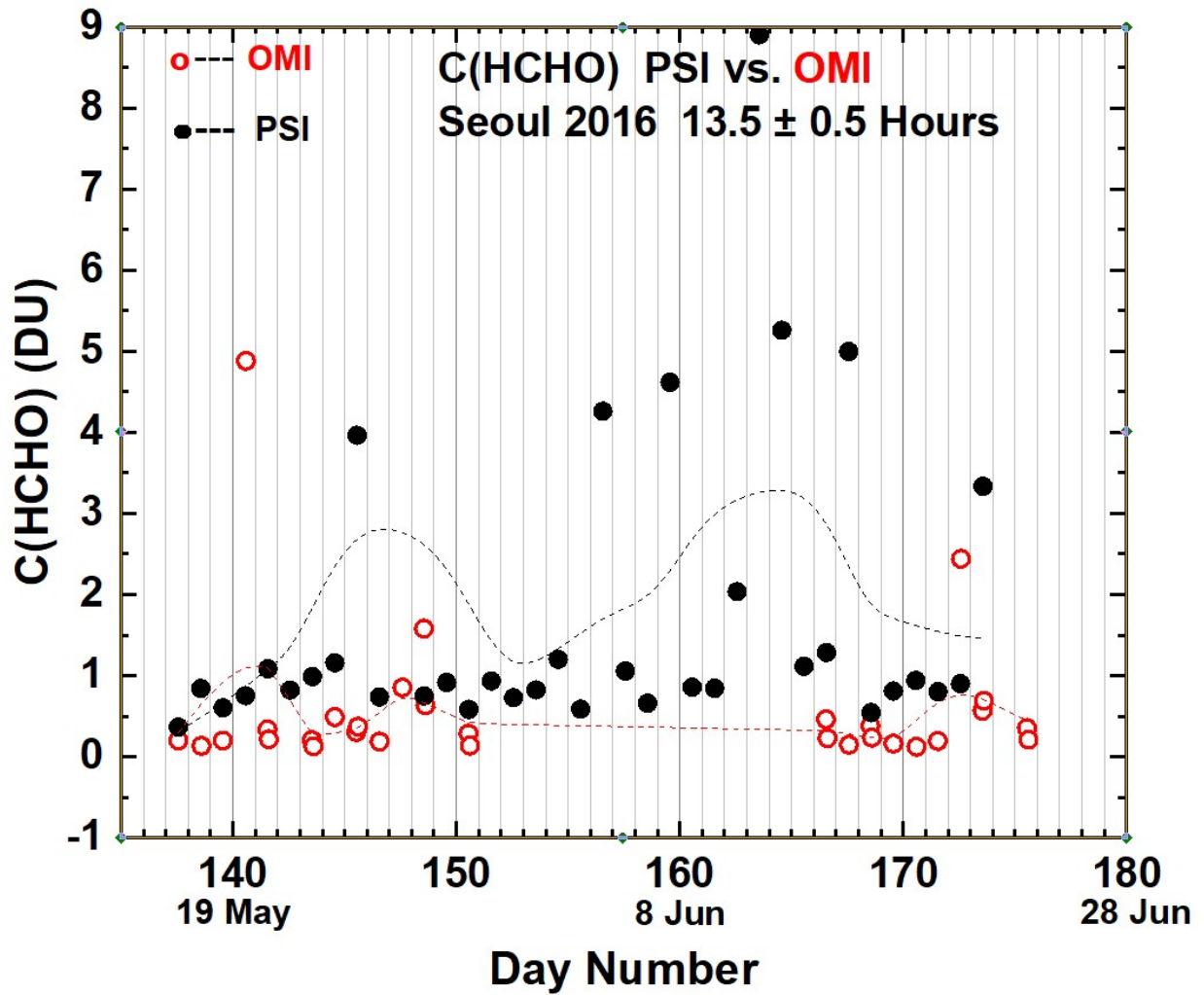


Fig. 21 Compare PSI • and OMI ◦ retrievals of C(HCHO) at  $13.5 \pm 0.5$  hours. OMI overpass data, V03, are from <https://avdc.gsfc.nasa.gov/index.php?site=1113974256&id=81>

946

947 **F21**

948

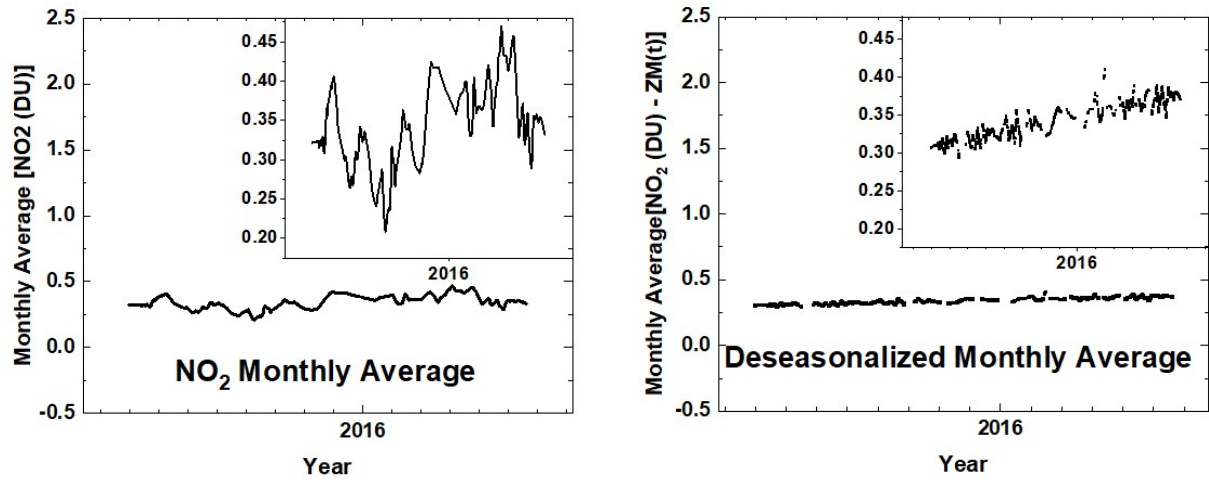


Fig. A1 An illustration of the deseasonalization (right panel) of the monthly running average of NO<sub>2</sub> (left panel) shown in Fig. 6. The insets are magnifications of the main plots.

949

950

951 **FA1**